Evolution of the Abundance of CO, O_2, and Dust in the Early Universe

David T. Frayer
National Radio Astronomy Observatory[1] and University of Toronto
Astronomy Department, University of Toronto, Toronto, Ontario, M5S 3H8
frayer@astro.utoronto.ca

Robert L. Brown
National Radio Astronomy Observatory, Charlottesville, VA 22903
rbrown@nrao.edu

ABSTRACT

We present a general set of calculations describing the chemical evolution of young massive galaxies and predict the evolution of the CO, O_2, and dust abundances as a function of age and metallicity. Over a wide range of input parameters, the models predict that (1) the total mass in gaseous metals peaks at early epochs ($z \sim 1-3$) when approximately half the total baryonic mass is in stars and half is in gas, (2) at its extreme, the mass of gaseous metals ranges from a few to more than ten times larger than the mass of gaseous metals at the current epoch, (3) due to the larger O/C ratios in chemically young systems, the O_2/CO ratio may be of order unity within dark molecular clouds at early cosmological epochs, and (4) at early epochs the global volume–weighted O_2/CO abundance ratios corrected for photodissociation are lowered significantly compared to the dark cloud solutions due to the lower metallicities and the higher UV fields. For a variety of models, we calculate the evolution of the mass of CO, O_2, and dust. We also compute the CO(1→0) and $O_2(1,1 \rightarrow 1,0)$ line intensities and the thermal dust emission as a function of redshift. The model calculations suggest that both redshifted thermal dust emission and CO line emission will be easily observable in young massive galaxies with the next generation of millimeter and submillimeter wavelength telescopes. Although more challenging, the O_2 lines may be observable in chemically young galaxies. Even though molecular oxygen has yet to be observed outside the solar system, and hence is much less abundant than CO in the Milky Way, the models indicate that O_2 may be significantly more abundant in the early stages of galaxy evolution.

Subject headings: early universe — galaxies: evolution — galaxies: formation — galaxies: ISM — ISM: molecules

[1]The National Radio Astronomy Observatory is a facility of the National Science Foundation operated under cooperative agreement by Associated Universities, Inc.

1. Introduction

Understanding the process of galaxy formation and the subsequent evolution is one of the most active areas of astronomical research, but our knowledge of the manner by which nascent gas forms stars and galaxies is still seriously incomplete. Since galaxies are expected to evolve quickly during the first Gyr (e.g., Tinsley 1972), observations of young galaxies are crucial for our understanding of the star formation and chemical evolutionary history of galaxies. Optical observations have revealed a plethora of information on young galaxies. Recently, a large population of star forming galaxies has been discovered at high redshift (Steidel et al. 1996). Studies of damped Lyα systems (Wolfe et al. 1986; Lanzetta et al. 1991) suggest that the total amount of neutral gas in these systems has decreased substantially from $z \simeq 3.5$ to $z \sim 0$, presumably due to the consumption of the gas via star formation (Lanzetta et al. 1995). Also, observations of the damped Lyα systems indicate that significant amounts of metals ($Z \sim 0.1 Z_{\odot}$ at $z \sim 2.5$, Pettini et al. 1994) and dust (Pei, Fall & Bechtold 1991; Fall & Pei 1993) are produced at early epochs. In fact, observations of the gas near some high redshift QSOs suggest abundances that are even in excess of solar (Petitjean, Rauch, & Carswell 1994; Turnshek et al. 1996). All of these optical results suggest that high redshift systems are already metal–enriched and at least some are undergoing extensive star formation.

In addition to the optical results, recent high–redshift CO and dust detections at mm and sub–mm wavelengths have confirmed the existence of copious amounts of metals at very early epochs (Brown & Vanden Bout 1991; Solomon, Downes, & Radford 1992; Barvainis et al. 1994a; McMahon et al. 1994; Chini & Krügel 1994; Dunlap et al. 1994; Isaak et al. 1994; Ivison 1995; Ohta et al. 1996; Omont et al. 1996a; Omont et al. 1996b). These CO and dust observations have the advantage of providing direct measurements of the mass of the gaseous reservoir from which the stars form. Such observations are crucial for constraining the evolutionary models for galaxies. Only by combining both optical and radio observations will we gain a complete picture of galaxy formation and evolution.

Despite the cumulative expenditure of many thousands of hours of telescope time by several groups in quest of high redshift CO and dust detections, there has yet to be a complementary investigation into the expected quantity and composition of the molecular gas and dust in young galaxies. In this paper we address these issues by studying the chemical evolution of the gas in massive galaxies undergoing large rates of star formation at early epochs, and we predict the evolution of the molecular gas and dust content.

In addition to the aforementioned CO and dust detections at high redshift, this theoretical investigation is motivated by several other observational results. From observations of nearby galaxies (Wilson 1995; Arimoto, Sofue, & Tsujimoto 1996), we are beginning to understand how metallicity affects the molecular abundances in chemically young galaxies. Furthermore, observations of nearby metal–poor galaxies with the Hubble Space Telescope (HST) have shown that the C/O ratio increases with metallicity (Garnett et al. 1995). This result has important

ramifications on the molecular composition of chemically young systems. In particular, the O_2/CO ratio decreases exponentially with increasing C/O ratios (Langer & Graedel 1989 [LG89]). One of the major goals of this paper is to investigate how variations of the C/O ratio affect the O_2/CO ratio at early cosmological epochs.

In order to calculate the chemical evolution of the gas in young galaxies, we formulate a numerical model (§2) based on the standard equations governing the chemical evolution of stars and gas in galaxies (Tinsley 1980). The solutions to these equations depend sensitively on (1) the initial mass function (IMF), which describes the fraction of stars formed at each initial stellar mass, (2) the stellar yields, (3) the parameters governing the star formation rate (SFR), and (4) the time scales for which gaseous systems collapse to form galaxies. The redshift corresponding to each time scale depends, of course, on the cosmological parameters. For all redshift scales in this paper, we adopt the standard Friedmann cosmology with $q_o = 1/2$ and $\Lambda = 0$. In such a universe, the age of a galaxy as a function of redshift is

$$T(z) = \frac{2}{3H_o}\left[\left(\frac{1}{1+z}\right)^{3/2} - \left(\frac{1}{1+z_f}\right)^{3/2}\right], \tag{1}$$

where z is the redshift of the galaxy and z_f is the redshift at which the galaxy forms (e.g., Fritze-v. Alvensleben et al. 1989). In this paper we use $z_f = 5$ (the redshift of the most distant known QSO; Schneider, Schmidt, & Gunn 1991) and $H_o = 80\,\mathrm{km\ s^{-1}\,Mpc^{-1}}$ (Pierce et al. 1994; Freedman et al. 1994).

The stellar yields, which quantify the amount of gaseous material returned into the interstellar medium (ISM) via supernovae, stellar winds, and planetary nebulae, are very important input parameters into the chemical evolutionary models. We use the stellar yields calculated as a function of metallicity for massive stars by Maeder (1992) [M92] and Woosley & Weaver (1995) [WW95]. The stellar yields are very dependent on supernova energies, mass loss via winds (M92), the masses of stellar remnants, and the parameters governing stellar nucleosynthesis, such as the mixing length parameter (Renzini & Voli 1981 [RV81]).

Since the properties of protogalaxies are still very uncertain, we develop a general set of models. By varying the above mentioned parameters, we calculate the gas mass, stellar mass, and metallicity as a function of age for 24 different models (§3). The models are loosely constrained by the observed properties of the Milky Way and by the abundances of nearby HII galaxies. We follow the evolution of the oxygen and carbon elemental species as well as the total metallicity (Z) since the molecular and dust abundances are sensitive to these quantities.

By combining the results of the chemical evolutionary models with previous detailed computations of gas–phase molecular chemistry (LG89; Millar & Herbst 1990 [MH90]), we predict the evolution of the O_2/CO ratio (§4). We discuss several scenarios explaining the apparent lack of O_2 in the local universe, and consider the implications for galaxies at earlier epochs. We calculate the evolution of the total mass contained within the CO, O_2, and dust species. These calculations

are sensitive to several uncertain parameters, such as (1) the fraction of gas in molecular form, (2) the fraction of molecular gas in dark cloud cores ($A_V \gtrsim 5$), (3) the evolution of the $N(\mathrm{CO})/\mathrm{N}(\mathrm{H_2})$ ratio, (4) the $M(\mathrm{H_2})$ to $L(\mathrm{CO})$ conversion factor as a function of metallicity and environment, (5) the effect that photodissociation has on the extent of the CO and O_2 emission regions, (6) the effect that turbulent mixing has on the molecular chemistry, (7) the relative depletion and subsequent chemistry of atomic and molecular species on grains, and (8) variations of the gas–to–dust ratio with metallicity. In addition, the models are calibrated using assumptions based on the properties and chemistry within Galactic clouds which may not necessarily be applicable for intense starburst systems. Given the uncertainties in these parameters, we present several scenarios comparing the dust and molecular gas content of the current epoch with that of the early universe. In §5 we compute the evolution of the intensities of the redshifted CO(1→0) and $O_2(1,1 \rightarrow 1,0)$ lines and the thermal dust continuum emission. Finally, we discuss the feasibility of observing these species at high redshift using current and future radio telescopes.

2. Chemical Evolution Model

2.1. Basic Equations

We use the formalism of Tinsley (1980) to solve the standard equations governing the evolution of gas and stars in galaxies. At all times the total mass in the system (M_T) is the sum of the gas mass M_g, the stellar mass M_s, and the total mass contained in stellar remnants M_r. These quantities are individually determined by solving the following set of time–dependent differential equations:

$$\frac{dM_T}{dt} = f(t), \tag{2}$$

$$\frac{d(M_s + M_r)}{dt} = \Psi(t) - E(t), \tag{3}$$

$$\frac{dM_g}{dt} = -\Psi(t) + E(t) + f(t). \tag{4}$$

The function $f(t)$ describes the net flow of material into or out of the system. In the case of inflow $f(t)$ is positive, and with net outflow $f(t) < 0$. The total consumption rate of the gas by star formation is represented by $-\Psi(t)$. The rate at which material is ejected back into the system from stars via supernovae, planetary nebulae, and stellar winds is

$$E(t) = \int_{m_t}^{m_u} (m - w_m)\Psi(t - \tau_m)\Phi(m)dm, \tag{5}$$

where w_m is the remnant mass of a star with an initial mass m, Φ is the IMF ($\Phi = dN/dm$), and τ_m is the lifetime of a star of mass m. The product $\Psi(t - \tau_m)\Phi(m)$ is the total number of stars of mass m formed at the time of their birth $(t - \tau_m)$. The lower limit of integration m_t is the stellar mass for which $\tau_m = t$, and m_u is the upper limit on the mass of a star. Equation (5) uses the

standard approximation that each star undergoes its entire mass loss at the end of its lifetime. Since this approximation fails on short time scales due to mass loss from stellar winds, we restrict analyses to time scales $t > 10^6$ yr. The production rate of stellar remnants is described by

$$\frac{dM_r}{dt} = \int_{m_t}^{m_u} w_m \Psi(t - \tau_m)\Phi(m)dm. \tag{6}$$

The rate of change of stellar mass dM_s/dt is solved directly by combining equation (3) and equation (6).

Analogous to equation (4), the time–dependent metal abundance Z_i of species i is represented by

$$\frac{d(Z_i M_g)}{dt} = -Z_i \Psi(t) + E_{Z_i}(t) + Z_{i_f} f(t), \tag{7}$$

where Z_{i_f} is the metallicity of the infalling or outflowing gas. The ejection rate of metals is

$$E_{Z_i}(t) = \int_{m_t}^{m_u} [(m - w_m)Z_i(t - \tau_m) + mp_{z_i}(m)]\Psi(t - \tau_m)\Phi(m)dm, \tag{8}$$

where $mp_{z_i}(m)$ is the stellar yield of metal Z_i from a star with initial mass m. In the above equation, we have made the correction suggested by M92 which removes a term from the formula given by Tinsley (1980) in order to conserve overall mass. This minor correction does not modify the widely used analytical solutions given by Tinsley.

2.2. Analytical Solutions

The instantaneous recycling approximation is often used to remove the time dependency from the differential equations in §2.1 which allow for simple analytical solutions. In this approximation stars above a certain mass value (e.g., $\sim 10\,M_\odot$) die immediately after birth and stars with masses less than this value live forever, so that $(t - \tau_m)$ can be replaced simply by t. In the case of the Closed Box Model, where $f(t) = 0$, and assuming that $M_g = M_T$ and $Z = 0$ at $t = 0$, it is straight forward to show (e.g., Tinsley 1980)

$$Z_i = y_i \ln(\mu^{-1}), \tag{9}$$

where μ is the gas fraction M_g/M_T. The net yield y_i is the mass of new metals of species i ejected by all stars per unit mass that is locked into stars and stellar remnants; it is given by

$$y_i = \frac{1}{(1 - R)} \frac{\int_{m_l}^{m_u} mp_{z_i}\Phi(m)dm}{\int_{m_l}^{m_u} m\Phi(m)dm}, \tag{10}$$

where the IMF is defined between the upper (m_u) and lower (m_l) stellar mass limits. The returned fraction R is the fraction of original stellar mass that has been ejected back into the system and is expressed by

$$R = \frac{\int_{m_l}^{m_u} [m - w_m]\Phi(m)dm}{\int_{m_l}^{m_u} m\Phi(m)dm}. \tag{11}$$

Traditionally, R and y_z have been the main parameters for studying galactic chemical evolution models since they depend on the adopted IMF and the stellar yields predicted by stellar evolution, but not on $\Psi(t)$.

Another popular analytical solution is the case of simple infall. The simple infall model assumes that the star formation rate is balanced with the rate of infall plus stellar gas loss so that the total *gas* mass remains constant with time. When instantaneous recycling is also assumed, the equations have the solution (Larson 1972)

$$Z_i = y_i[1 - e^{(1-\mu^{-1})}]. \tag{12}$$

Other more complicated infall solutions can be found in Clayton (1987). Solutions including the effects of galactic winds ($f(t) > 0$) are discussed by Matteucci & Chiosi (1983), and a general set of equations representing both gaseous inflow and outflow is given by Edmunds (1990).

The instantaneous recycling approximation, which permits these simple analytical solutions, is generally not valid in cases where the SFR is strongly time dependent since $\Psi(t - \tau_m) \neq \Psi(t)$. Also, the time–dependent ratios of metal abundances are determined incorrectly when ignoring stellar lifetimes since heavy elements are produced in different quantities in stars with different lifetimes (i.e., different masses). Equally important, it is impossible to derive information on the earliest stages of evolution since the approximation is only valid when studying effects which vary on time scales much larger than the lifetimes of massive stars ($\gg 10^7$ yr).

2.3. Numerical Solution

We numerically solve the equations of §2.1 to avoid the necessity of using the instantaneous recycling approximation. We follow the evolution of the gas using a time step of 2×10^6 yr. Numerical solutions of the basic evolutionary equations are very general and have been used extensively to investigate many astrophysical questions (e.g., Matteucci & Tornambè 1987; Rana 1991; Timmes, Woosley, & Weaver 1995). In this paper we solve these equations in order to study the evolution of carbon, oxygen, and total metallicity in young galaxies. Since the characteristics of young galaxies are uncertain, we vary the input parameters to understand how the results are modified with changing inputs. In Table 1 we summarize the values of the input parameters for 24 different models, covering the range of likely astrophysical parameters. We discuss particular details of these parameters in the following subsections.

2.3.1. The IMF, the Star Formation Rate, and Infall Parameters

The solutions to the equations governing the chemical evolution of galactic systems depend sensitively on the adopted IMF, the star formation history, and the rate of gaseous inflow or

outflow. We adopt a single slope power–law approximation to the IMF of the form

$$\Phi(m) \propto m^{-(1+x)}, \tag{13}$$

where x is the slope of the IMF. We compare the results of a Salpeter power law ($x = 1.35$, Salpeter 1955) with those of a steeper ($x = 1.7$) IMF and a flatter IMF ($x = 1.1$). In the equations of §2.1, the IMF is normalized such that

$$\int_{0.08\,M_\odot}^{m_u} m\Phi(m)dm = 1, \tag{14}$$

where m_u is the upper limit to the mass of a star. The calculations of WW95 include stars as massive as $m_u = 40\,M_\odot$, while the calculations of M92 include stars with mass up to $m_u = 120\,M_\odot$.

To test the dependency on the star formation history, we use a simple power law for the star formation rate of the form (Schmidt 1959)

$$\Psi(t) = \nu M_T(t)[\mu(t)]^n. \tag{15}$$

The exponent is varied such that the dependence on the gas fraction is between linear and quadratic; we use the values of $n = 1.0$, 1.5, and 2.0. In studying of the evolution of elliptical galaxies, Matteucci & Tornambé (1987) adopt $n = 1$. Alternatively, for spiral galaxies Dopita & Ryder (1994) find that the values of $n \simeq 1.5 - 2$ are consistent with observations. We vary the efficiency factor between the values $\nu = 0.5$, 2, and 5 Gyr^{-1}. In studying Galactic chemical evolution, Timmes et al. (1995) find that $\nu = 2.8$ Gyr^{-1} is the best fit to the observational data. Even though surface densities may be more directly related to the SFR (e.g., in terms of the Toomre stability criterion for disks; Kennicutt 1989), we use total masses instead of mass surface densities in equation (15). The advantage of using this formalism is that we do not need to adopt a particular dynamical model or geometry (e.g., disk or spheroid). By using total masses, we only determine the total global SFR. Granted, this approximation over simplifies the actual picture of star formation in galaxies which may differ considerably from ellipticals and spirals and undoubtedly includes interactions and mergers, but the approximation is suitable for studying global properties over long time scales ($t \gtrsim$ Gyr). For example, in the Galactic disk where $M_T \sim 10^{11}\,M_\odot$ and $\mu = 0.1$ (Rana & Basu 1992), we find that equation (15) implies that the $SFR \sim 6\,M_\odot\,\mathrm{yr}^{-1}$, using $n = 1.5$ and $\nu = 2$ Gyr^{-1}. This value compares well with the Galactic estimate of the $SFR \simeq 5\,M_\odot\,\mathrm{yr}^{-1}$ (e.g., Mezger 1987). Extrapolating back to earlier epochs where μ could be of order unity, the most massive galaxies ($M_T \sim 10^{12}\,M_\odot$) are expected to have total star formation rates of order $10^3\,M_\odot\,\mathrm{yr}^{-1}$.

We study the numerical solutions for both the closed box models ($f(t) = 0$) and infall models ($f(t) > 0$). For the infall models, we assume that the initial mass is zero and that the accreting gas is primordial ($Z_{i_f} = 0$ in eq. [7]). To describe the infall rate, we use an exponential function

$$f(t) = \frac{M_T(t \to \infty)}{\tau_f} \exp(-t/\tau_f), \tag{16}$$

where $M_T(t \rightarrow \infty)$ is the maximum mass of a system as $t \rightarrow \infty$ and the time scale for formation is τ_f. We have chosen $M_T(t \rightarrow \infty) = 10^{12}\, M_\odot$ since massive galaxies are more readily observable at high redshift. For galaxies with smaller masses, the results presented in this paper may be scaled accordingly. In the formation of a thin disk, Burkert, Truran, & Hensler (1992) find that $\tau_f \simeq 4$ Gyr. Spheroidal systems are expected to form on shorter time scales ($\tau_f \sim 1$ Gyr; Theis, Burkert, & Hensler 1992). In this paper, we vary τ_f between the values of 1, 2, and 4 Gyr. For the limiting cases of $\tau_f \rightarrow 0$ or $\tau_f \rightarrow \infty$, we recover the closed box model solution ($f(t) = 0$).

2.3.2. Stellar Yields and Lifetimes

Stellar yields are arguably the most important input parameters governing the evolution of elemental abundances. In order to include the dependency of the stellar yields as a function of metallicity, we adopt the yields from massive stars based on the calculations of WW95 and M92. Woosley and Weaver determined the ejected masses resulting from Type II supernova models of varying initial stellar masses ($12 \leq M/\, M_\odot \leq 40$) and varying initial metallicities (0, 10^{-4}, 0.01, 0.1, and 1.0 $Z_\odot$). Their calculations do not include pre–supernova mass loss. The ejected yields in massive stars depend on the energy of the supernova explosion. Simply stated, energetic explosions return more material to the ISM than less energetic explosions which tend to leave more massive stellar remnants. We adopt the yields from the models using intermediate (Case B) and large (Case C) supernova energies (WW95). For the purposes of our calculations, we linearly interpolate the stellar yields and the masses of the stellar remnants for intermediate metallicities. For metallicities larger than solar, we use the yields calculated for solar metallicity.

Maeder's models, on the other hand, do include mass loss by stellar winds prior to the supernova event. To assess these effects, we use the yields and remnant masses of M92. Maeder has shown that mass loss in massive stars leads to stellar yields that are highly sensitive to the initial metallicity. For massive stars ($M > 25\, M_\odot$) the oxygen yields are expected to decrease with metallicity due to the winds, whereas the carbon yields increase with metallicity. These tendencies are expected since massive stars at high metallicity have sufficiently high opacities, such that large amounts of helium and carbon are ejected into the ISM before being processed into heavier elements. This produces a low oxygen yield and a high carbon yield. The reverse is expected at low metallicities. Since at low metallicities the opacity is low and mass loss is less important, most of the new helium and carbon can be processed further into heavier elements prior to the supernova event. The resulting ejecta have a high oxygen yield and a low carbon yield. Unlike the yields of WW95 which cover a complete grid of metallicities, the yields of M92 are only for $Z = 0.001$ and $Z = 0.02 \simeq Z_\odot$. We avoid extrapolations and use the yields at $Z = 0.001$ for $Z \leq 0.001$, the yields at $Z = 0.02$ for $Z \geq 0.02$, and linearly interpolate for intermediate metallicities. As pointed out by Prantzos, Vangioni–Flam, & Chauveau (1994), the stellar yields for $Z < 0.001$ are expected to be similar to those at $Z = 0.001$ since mass loss is already negligible at this metallicity.

In Figure 1 we show the expected stellar yields for massive stars from the work of WW95C

(Case C) and M92 at solar ($Z_\odot = 0.02$) and subsolar metallicities. At low metallicities, the yields of both M92 and WW95C are similar. The ratio of the oxygen to carbon yields increases as a function of stellar mass, a simple reflection of the fact that more massive stars burn more carbon into oxygen than less massive stars. Since massive stars have the shortest lifetimes, these results indicate that we should expect an excess of oxygen relative to carbon at the earliest epochs. At high metallicities, Figure 1 shows how the inclusion of winds substantially modifies the resulting yields. Without stellar winds massive stars have yields of $mp_O/mp_C > 1$, whereas if winds are included then metal–rich massive stars ($M > 25\,M_\odot$) become an important source of carbon ($mp_O/mp_C < 1$; M92). Therefore, the stellar winds in massive stars tend to amplify the carbon abundance relative to oxygen as a function of increasing age and metallicity.

For low and intermediate mass stars ($1 \leq M/\,M_\odot \leq 8$), we use the stellar yields from RV81. We use the yields predicted with a mass loss parameter of $\eta = 0.33$ and with the mixing length ("hot–bottom" burning) parameters of $\alpha = 1.5$ and $\alpha = 0$ given for $Z = 0.02$ and $Z = 0.004$ (RV81). As with the yields of M92, we linearly interpolate for intermediate metallicities. We use the yields and remnant masses at $Z = 0.004$ for $Z \leq 0.004$ and the yields and remnant masses at $Z = 0.02$ for $Z \geq 0.02$. The relative yields of C, O, and N are extremely sensitive to the mixing length parameter for intermediate mass stars ($4 \lesssim M/\,M_\odot \lesssim 8$). In the case of $\alpha = 0$ (no "hot–bottom" burning) the carbon yield dominates, whereas for $\alpha = 1.5$ nitrogen production is important. Correspondingly, the mixing length parameter affects the epoch at which intermediate mass stars are significant sources of carbon enrichment. For $\alpha = 1.5$, only stars less massive than $5\,M_\odot$ are expected to contribute significantly to the carbon yields, suggesting a relevant time scale of $\sim 10^8\,$yr. For $\alpha = 0$, however, the more massive intermediate mass stars are an important carbon source, decreasing the relevant time scale to only $\sim 10^7\,$yr. Recent work by Chieffi, Straniero, & Salaris (1995) suggest that the mixing length parameter is $\alpha \simeq 1.6$ for low metallicity stars ($Z \sim 0.01 Z_\odot$) and increases to $\alpha \simeq 1.9$ for stars of intermediate metallicity. In this paper we concentrate on the models using $\alpha = 1.5$ and do not include the possible increase of α with metallicity.

We have ignored the contribution of Type I supernovae to the stellar yields since Type I events produce mostly Fe and Ni species and only a little carbon and oxygen. More importantly, Timmes et al. (1995) have shown that the Type I contribution is relatively small compared to yields from single star evolution. Using the amplitude of Type I contributions as a free parameter and comparing with Galactic abundance observations, they estimate that the Type I contribution is only 0.007 times that of the contribution from single stars over the mass range of $3\,M_\odot$ to $16\,M_\odot$ (the minimum and maximum binary mass which produces a carbon–oxygen white dwarf).

We use the stellar lifetimes from Theis et al. (1992):

$$\tau(m) = \begin{cases} 1.2 \times 10^{10} (\frac{m}{M_\odot})^{-2.78}\,\mathrm{yr} & m < 10\,M_\odot \\ 1.1 \times 10^{8} (\frac{m}{M_\odot})^{-0.75}\,\mathrm{yr} & m \geq 10\,M_\odot. \end{cases} \tag{17}$$

As with the stellar yields, the stellar lifetimes also vary with metallicity. However, these differences

are most important for low mass stars. For low mass stars at high metallicity, the opacities are larger so the luminosities are lower, hence, producing longer lifetimes. For a $3\,M_\odot$ star the lifetime differences are about 20% between the cases of $Z = 0.001$ and $Z = 0.02$, and for $M < 1\,M_\odot$ the differences are expected to be larger than 50% (Schaller et al. 1992). Since we are primarily concerned with massive stars at early times, our main results are insensitive to these differences.

3. Results of Chemical Evolution

The parameters of Table 1 were varied around the intermediate values of $x = 1.35$, $\nu = 2$, and $n = 1.5$ which represent typical values for galaxies at the current epoch. We have studied models using the yields of WW95 and M92 to test the importance of stellar winds. In Figure 2 we show the evolution of gas mass, stellar mass, total mass, and metallicity as a function of age for a typical closed box model, while Figure 3 displays the same quantities for an infall model. Since we are studying global properties, the derived metallicities represent a mass weighted average for the entire galactic system. For the Galactic disk, which has a metallicity gradient that ranges from $Z \sim Z_\odot$ in the solar neighborhood to $Z \sim 5Z_\odot$ in the central regions (Pagel & Edmunds 1981), the average metallicity is larger than solar.

In Figure 4 we present the evolution of gaseous metals $Z\mu$ as a function of age for several different parameters governing the SFR. For the parameters chosen in these models, the peak of gaseous metals as a fraction of the total mass occurs fairly rapidly, generally within ~ 2 Gyr. After which, the amount of gaseous metals decreases as the gas is consumed by the ongoing star formation and locked into low mass stars and stellar remnants. The consumption rate of the gas is, of course, very sensitive to the adopted star formation rates. For $n > 1$ the SFR decreases faster than the gas fraction, permitting a slow decline in the fractional amount of gaseous metals. Similarly, decreasing ν also decreases the SFR and reduces the consumption rate of gaseous metals. This parameterization of the SFR could be used to represent galaxies of different morphological types. Early–type galaxies, such as ellipticals and S0 galaxies, currently have little gas, suggesting high ν and low n. Alternatively, gas–rich, late–type spiral galaxies could have low ν and high n (Sandage 1986).

In Figure 5 we plot the mass of gaseous metals as a function of the gas fraction μ. The SFR parameters have little effect on the shape or maximum value of the curves, but they do determine the time scale for which a system will evolve to a given M_g/M_T. Although the shape of the curves is also basically independent of the IMF, the maximum amount of gaseous metals is extremely sensitive to the slope of the IMF. For a steep IMF, there are fewer massive stars so less metals are produced. Alternatively for a shallow IMF, more metals are produced. Since the maximum amount of gaseous metals is relatively insensitive to the SFR parameters, the IMF for these models can be constrained by comparing the implied net yields with previous studies. For the analytical solution of the closed box model (eq. [9]), the maximum amount of gaseous metals occurs at $\mu = 1/e = 0.368$ (Bally, Shull, & Hamilton 1993) and the implied net yield is $2.72(Z\mu)_{max}$. For

an IMF with $x = 1.35$ (Run 1), the implied net yield is $y_z = 0.025$, which is well within the range of values estimated for our Galaxy: $y_z = 0.036$ (Pagel 1987) and $y_z = 0.011$ (Rana 1991). For $x = 1.1$ (Run 2) and $x = 1.7$ (Run 3), the implied net yields are outside the range of acceptable Galactic estimates (Table 2), suggesting that the Salpeter IMF is an adequate approximation for describing the evolution of the Galaxy.

In Figure 6 we compare the numerical solutions to the analytical solutions given in §2.2. The analytical solution of the closed box model (eq. [9]) was plotted using a net yield of $y_z = 0.025$, which is the implied net yield for the closed box numerical solution of Run 1. For the infall models, the maximum $Z\mu$ occurs at $\mu \simeq 0.47$, which is at an earlier age than the maximum $Z\mu$ of the closed box models. For the analytical solution of the simple infall model (eq. [12]), we find that the implied net yield is $3.15(Z\mu)_{max}$, which corresponds to $y_z = 0.024$ for the numerical infall solution of Run 11. The consistency between the analytical and numerical solutions in Figure 6 is somewhat remarkable considering that the actual net yield for the numerical models changes with metallicity as the individual stellar yields change (eq. [10]), whereas for the analytical solutions the net yield is assumed to be constant. As expected, when the infall rate $f(t) \rightarrow 0$ in the numerical infall model, the solution deviates from that of the analytical infall model and approaches the solutions of the closed box models. The primary significance of these results on the evolution of gaseous metals is straightforward. Basically independent of the details of the model, the total mass of metals in the ISM of galactic systems is predicted to peak at early epochs ($z \sim 1 - 3$) when the total gas mass is similar to the total stellar mass.

Although understanding the evolution of metallicity is important, comprehending the evolution of the C/O ratio is more interesting and important for this study, since the molecular abundances are very sensitive to this ratio. As discussed in §2.3.2, low–metallicity massive stars produce more oxygen than carbon. Since the bulk of the carbon production occurs at later epochs, either from intermediate and low mass stars and/or from the winds of metal–rich massive stars, the gaseous C/O ratio is expected to increase with metallicity. Abundance determinations of Galactic stars are consistent with these expectations. In addition, extragalactic observations with the HST have provided similar results for HII galaxies (Garnett et al. 1995). In Figure 7 we plot the observed C/O abundance ratios along with the solutions of several models calculated for a variety of input parameters. The metallicities of the stars observed by Tomkin et al. (1992) and Clegg, Lambert, & Tomkin (1981) are determined from their Fe abundances, while the metallicities of the extragalactic sources observed by Garnett et al. (1995) are determined from the oxygen abundances, assuming the solar relationship of $Z = 23(\mathrm{O/H})$ (Grevesse & Anders 1989). At the low metallicities, the solutions based on the yields with the largest supernova energies (M92 and WW95C) better match the observations than the case of lower supernova energies (WW95B). The M92 solution with $m_u = 40\,M_\odot$ is similar to the WW95C solution which also uses $m_u = 40\,M_\odot$. With the M92 models, changing the mixing length parameter from $\alpha = 0$ to $\alpha = 1.5$ has little effect, indicating that most of the carbon is produced by the stellar winds from massive stars with $Z \gtrsim 0.1Z_\odot$. Previously, Prantzos et al. (1994) have accounted for the rise of the C/O ratio in

the disk of our Galaxy using the yields of M92 without requiring a significant contribution from intermediate and low mass stars. Using calculations based on the yields of WW95, however, the resulting abundances are sensitive to α because in these models the intermediate mass stars are the primary source of carbon.

In Figure 8 we further demonstrate the dependency of the C/O ratio as a function of metallicity on other parameters such as the adopted IMF, star formation history, and infall rate. Changing the exponent of the SFR power law (n) affects the solutions only slightly; n just determines the time scale for which a certain metallicity is reached. Lowering the efficiency parameter ν shifts the solutions to slightly lower metallicities. Similarly, steepening the IMF shifts the curves to lower metallicities and larger C/O ratios since fewer massive stars are produced.

By using the properties of galaxies at the current epoch, we can constrain many of the free parameters in the models. To be consistent with the net yields derived for the Galaxy, we choose models with $0.011 \leq y_z \leq 0.036$. For the closed box models, the implied net yields are $y_z = 2.72(Z\mu)_{max}$, while for the infall models $y_z = 3.15(Z\mu)_{max}$. As a second constraint, we use the relationship found by Garnett et al. (1995): $\log(\mathrm{C/O}) \propto \mathrm{B}\log(\mathrm{O/H})$, where $B = 0.43 \pm 0.09$ over the metallicity range of $-4.64 \leq \log(\mathrm{O/H}) \leq -3.6$ ratio. An additional constraint is the value of the O/C ratio at the lowest metallicity data point of Garnett et al. (1995): $6 \leq \mathrm{O/C} \leq 13$ at $\log(\mathrm{O/H}) = -4.64$. Using the metallicities and gas fractions of typical massive spiral galaxies in the local universe, we adopt $1 \leq Z/Z_{\odot} \leq 5$ and $0.01 \leq \mu \leq 0.1$ as the fourth and fifth constraints. In Table 2 we list the computed values of these 5 constraints for each of the models. Only the infall models of M92 (Run 10, 11, & 12) and the closed box model with $\alpha = 0$ (Run 5) satisfy all 5 of the constraints. Current stellar evolutionary theories argue for values of $\alpha \gtrsim 1.5$ (e.g., Chieffi et al. 1995), so the $\alpha = 0$ models are most likely not realistic and are included in this study mainly for comparison purposes. Hence, these results indicate that infall models using the stellar yields of M92 best fit the observed properties of the Milky Way. These results are consistent with the models of Prantzos et al. (1994) and Carigi (1994) which also addressed Galactic chemical evolution using the yields of M92. Unlike the models based on the yields of M92, the models based on the yields of WW95 do not predict the observed evolution of the C/O ratio with metallicity found for HII galaxies. These results underscore the importance of stellar winds, which are neglected in the WW95 yields, on the specific issue of the evolution of the C/O ratio. Although the WW95 models are not well tailored to understanding the evolution of the C/O ratio, these models do equally as well as the M92 models in describing the evolution of the metallicity and the gas fraction. In comparison with previous work, we find that the model parameters of Run 24, which are similar to the values used by Timmes et al. (1995), yield consistent results.

In Table 3 we list the time it takes for the models to achieve interesting stages of evolution. We include the age at which one half of the final total baryonic mass is in stars and stellar remnants ($\tau^*_{1/2}$), the age at which ZM_g is a maximum, and the age at which the system reaches solar metallicity. Generally, solar metallicity is achieved after $\tau^*_{1/2}$. However, for the infall models using the yields of M92, solar metallicities are achieved before $\tau^*_{1/2}$ and before the peak of gaseous

metals. In summary, all three of these epochs occur at a similar time for each of the models and occur roughly within the first 2 Gyr. Granted, not all galaxies evolve this quickly. Dwarf galaxies (Hunter & Gallagher 1985) and low surface brightness galaxies, such as Malin 1 (Impey & Bothun 1989), certainly do not. The models given in this paper are more representative of massive galaxies which undergo prodigious star formation at early times.

The current observations and the results of these modeling efforts are certainly not sufficient to determine a unique solution governing chemical evolution. However, this is not the goal of our work. The principal motivation behind these studies has been to determine the general evolution of carbon, oxygen, and metallicity and how this evolution is affected by varying input parameters. The basic results are summarized below. The models are consistent with the observations and predict that oxygen should be much more abundant than carbon at early epochs (O/C$\gtrsim$ 10). The evolution of carbon lags behind that of oxygen since it is produced at later times, from intermediate–low mass stars and from the winds of metal–rich massive stars. In addition to a different composition, the ISM of young galactic systems should contain a mass of gaseous metals which is greater than that found at the current epoch where the gas has been depleted due to star formation. Using these basic results, we now shift our attention to the molecular gas content of young galactic systems.

4. Molecular Chemistry

The models calculating the gas–phase abundances within dark molecular clouds consist of a sophisticated network of order one thousand time–dependent chemical reactions (Prasad & Huntress 1980; Graedel, Langer, & Frerking 1982; Herbst & Leung 1986 [HL86]; Herbst & Leung [HL89]; LG89; MH90). These models are sensitive to a variety of parameters such as the density, temperature, ionization field, and the initial chemical composition. However, the dominate parameter for determining the relative abundances of the carbon and oxygen species is the gas–phase carbon to oxygen ratio, $(C/O)_g$ (LG89). In Figure 9, we show the computed abundances of the C, O, O_2, and CO species as a function of the C/O ratio at approximately solar metallicity for the steady–state solutions of LG89. This figure demonstrates several important tendencies. The O_2/H_2 ratio is extremely sensitive to the $(C/O)_g$ ratio, while the CO/H_2 ratio is relatively constant. For high $(C/O)_g$ ratios, there is virtually no molecular oxygen since most of the free oxygen combines with carbon to form CO. For $(C/O)_g \lesssim 0.5$, there is an excess of oxygen after the formation of CO which may combine to produce O_2.

4.1. The Abundance of O_2 in the Local Universe

Molecular oxygen has yet to be detected conclusively outside the solar system despite the efforts of several observers. Due to atmospheric attenuation, Galactic studies have been limited to

searches of the rarer isotope $^{16}O^{18}O$, which have provided upper limits of $O_2/CO \lesssim 0.1$ (Liszt & Vanden Bout 1985 [LV85]; Goldsmith et al. 1985; Combes et al. 1991 [C91]; Fuente et al. 1993; Maréchal et al. 1997). Extragalactic searches for the redshifted 118.75 GHz $^{16}O_2$ emission line ($z \gtrsim 0.03$) have provided more sensitive limits, but they also have been unsuccessful (Liszt 1985, Goldsmith & Young 1989 [GY89], C91, Liszt 1992 [L92]). Recently, Combes & Wiklind (1995) have reported a very sensitive nondetection of O_2 ($N(O_2)/N(CO) < 0.014$) from an absorption line experiment toward a background mm–wavelength continuum source. The current most stringent observational limit is $N(O_2)/N(CO) < 0.01$ for the $z = 0.026$ galaxy NGC 6240 (C91).

If the gas–phase C/O ratio is similar to the solar ratio of C/O$\simeq 0.4$, then the observed upper limits of the O_2/CO ratio are less than the values predicted by the steady–state theoretical models ($O_2/CO \sim 0.5$). Several ideas have been put forth to explain this inconsistency. These ideas can be divided into two broad classes: (1) deviations of gas–phase abundances from solar; and (2) limitations of the gas–phase steady–state chemistry models.

Perhaps the solar C/O ratio is not typical within the molecular gas clouds previously searched for O_2. If the gas–phase C/O ratio is increased by only a factor of 2, all of the observational upper limits of O_2 are consistent with the steady–state expectations. For example, the average value of the C/O ratio determined by several measurements within the Orion Nebula is $C/O = 0.71 \pm 0.18$ (Meyer et al. 1994 (M94) and references therein). The solar C/O ratio is also smaller than the value of C/O ~ 0.6 predicted from extrapolating the relation found by Garnett et al. (1995). One of the difficulties in directly comparing the C/O ratio and the O_2/CO limits is that the elemental abundances are determined by absorption lines through the diffuse ISM toward stars, stellar abundances, or from the studies of HII regions. The abundances within the dense molecular regions may be significantly different. In any case, the C/O ratio is not constant within the ISM, and typical measurements range between C/O $\sim 0.4 - 0.8$ (e.g., Cardelli et al. (1993) [C93]). These differences may arise due to local environmental conditions. For example, the Sun may have formed in the late stages of the life of its parent molecular cloud, and the solar abundances may have been enriched from earlier supernovae within the cloud (Cunha & Lambert 1994). Since supernova ejecta from massive stars are more abundant in oxygen than in carbon (§ 2.3.2), the solar C/O ratio may be lower than the typical ISM abundance ratio.

The situation is even less clear for extragalactic measurements where the physical conditions and chemical properties could vastly differ from Galactic clouds. The extragalactic searches for O_2 have concentrated on the bright cores of CO–rich star–forming galaxies. These central regions of the galaxies are expected to have at least roughly solar metallicity and could possibly have metallicities as large as $5Z_\odot$ (e.g., Pagel & Edmunds 1981). Since C/O varies roughly as $Z^{1/2}$ (§3), the carbon to oxygen ratio is expected to be larger than solar. For the galaxy NGC 7674, Kraemer et al. (1994) [K94] find that the best model fit to their IUE spectra suggests that C/O$\sim 3/2$. Therefore, it is not surprising that O_2 was not observed in this source by L92. If similarly large C/O ratios are found for the center of other galaxies, then the observational deficiency of extragalactic O_2 in the local universe would not contradict the theoretical estimates.

An additional method suggested for increasing the gas–phase C/O ratio involves the selective depletion of oxygen (C91). Several mechanisms have been proposed for excess oxygen depletion. The gas phase oxygen abundance may be depleted by large quantities of solid H_2O, CO_2, CO, O_2, and silicates on the mantles of grains (d'Hendecourt & Jourdain de Muizon 1989; Ehrenfreund et al. 1993; de Graauw et al. 1996; Whittet et al. 1996). Since both CO and O_2 have similar binding energies to the dust grains, these species are expected to have similar levels of depletion onto grain surfaces (Bergin, Langer, & Goldsmith (1995) [BLG95]). Barring any additional effects, the gaseous O_2/CO ratio would remain roughly constant as depletion increases. Blake et al. (1987) suggests that even if C and O are adsorbed at equal rates onto grains to form primarily CH_4 and H_2O, respectively, the nonpolar CH_4 molecule will evaporate more easily than the polar H_2O molecule, resulting in larger gas–phase C/O ratios. However, observations are inconsistent with large H_2O abundances. Only 10% of the oxygen is contained within solid H_2O in dense clouds (Smith, Sellgren, & Brooke 1993), and even less is contained within gaseous H_2O. Using observations with the Kuiper Airborne Observatory, Zmuidzinas et al. (1996) conclude that much less than one percent of the oxygen is in gaseous H_2O within the cool quiescent molecular envelopes. In hot molecular cores, only a few percent of the oxygen is in gaseous H_2O (Zmuidzinas et al. 1996; Gensheimer, Mauersberger, & Wilson 1996; van Dishoeck & Helmich 1996), which is consistent with the evaporation of solid H_2O from the grain mantles or may suggest the importance of high temperature gas–phase chemistry (van Dishoeck & Helmich 1996). In any case, current observations do not support the scenario of excess oxygen depletion as a mechanism for significantly increasing the C/O ratio with respect to the solar value.

If the solar C/O ratio is the typical gas–phase value within molecular clouds, then the most likely reason for the observational deficiency of O_2 involves limitations in the gas–phase steady–state chemistry models. More recent models have included grain surface adsorption and desorption (BLG95) and have included reactions on the surfaces of grains (Hasegawa & Herbst 1993; Willacy & Williams 1993). Unfortunately, the steady–state solutions of these models still have difficulties explaining the observed molecular abundances. In particular, the models that include networks of reactions on grain surfaces vastly under produce the gas–phase molecular abundances in dense clouds. Observations of the dense Taurus region have shown that only 5% to 40% of the total number of CO molecules exist on grains (Whittet 1993) with a gas phase abundance ratio of $CO/H_2 \sim 10^{-4}$ (Frerking, Langer, Wilson 1982), whereas surface chemistry models predict much lower gas–phase abundances (e.g., $CO/H_2 \sim 10^{-9}$; Hasegawa & Herbst 1993). Models that neglect surface reactions, but include adsorption and desorption, do a much better job of yielding sufficient quantities of gas–phase CO (BLG95). However, the models of BLG95 predict similar levels of depletion for CO and O_2, and the resulting O_2/CO ratio does not vary from the gas–phase chemistry models of LG89 and MH90 (Fig. 10). Therefore, grain chemistry models, by themselves, cannot currently explain the apparent deficiency of O_2 in Galactic clouds.

An alternative explanation for the observed deficiency of O_2 may involve turbulent diffusion and mixing (Xie, Allen, & Langer 1995 [XAL95]; Chièze & Pineau des Forêts 1989; Pineau des

Forêts, Flower, & Chièze 1992) [PFC92]). Mixing of dense interior gas with the outer layers prevents the clouds from reaching their steady–state solutions ($t > 10^7$ yr), resulting in solutions similar to those found at earlier times ($t \sim 10^5$ yr; e.g., MH90; HL89). For these models the atomic carbon abundances are much larger, and the O_2 abundances can be lowered by several orders of magnitude. The O_2 abundance is extremely sensitive to the abundance of atomic carbon since the O_2 molecules are destroyed by atomic carbon to form CO. The carbon atoms also compete with the oxygen atoms in reacting with OH molecules, which decreases the rate of O_2 formation. The observations of the atomic carbon lines in M82 (Schilke et al. 1993; Stutzki et al. 1997) and NGC 253 (Harrison et al. 1995) suggest enhanced atomic carbon abundances in these nearby starburst systems. The high atomic carbon abundances may result from a turbulent, clumpy medium where the clouds are repeatedly exposed to UV radiation (Stutzki et al. 1997), possibly suggesting the applicability of mixing scenarios and the early–time solutions. The situation could be vastly different for chemically young galaxies where the O/C$\gg 1$. For O/C$\gtrsim 10$, the total carbon abundance is lowered sufficiently such that the early–time solutions are expected to be similar to the steady–state solutions (Fig. 10).

In Figure 10 we show the O_2/CO ratio as a function of the O/C ratio computed by many theoretical models as well as the current observational limits. For the LG89 and MH90 models, the gas–phase steady–state solutions are for molecular clouds with large values of extinction ($A_V \sim 10$). The dark cloud solutions of LG89 and MH90 are fitted by the following function:

$$\log\left(\frac{O_2}{CO}\right) = -0.357 + 0.957\log\left(\frac{O}{C}\right) - 1.426\left(\frac{C}{O}\right)^2. \quad (18)$$

The coefficients are determined by a singular value decomposition least–squares fit to the data (Press et al. 1986). In the limit as O/C $\rightarrow \infty$, equation (18) conserves the number of total oxygen atoms and has the correct dependency on the O/C ratio [O_2/CO $\lesssim 1/2$(O/C); LV85]. Equation (18) fits remarkably well to the data of LG89 and MH90 (see Fig. 10), even though the LG89 solutions are for Galactic clouds, while the solutions of MH90 are for clouds in the LMC and SMC which have lower input metallicities and higher UV radiation fields. From these results we deduce that the O_2/CO ratio is primarily determined by the O/C ratio and does not depend significantly on the metallicity within dark clouds. All of the other theoretical points in Figure 10 are normalized to the data of LG89 and MH90 using their respective steady–state solutions. The fit displayed for the early–time solutions is made using only the data of MH90 and has the same functional form as equation (18). The uncertainties in the O/C ratio for NGC 6240 and the galaxies of L92 and GY89 are estimated by assuming that these galaxies have a central metallicity of $Z/Z_\odot = 2\pm\ ^{3}_{1.5}$ and that $Z \propto (C/O)^2$ (§3). For the molecular regions of ρ Oph, we adopt the O/C ratio derived toward ζ Oph as a "typical" ISM value (C93), and this ratio may not be applicable for ρ Oph.

4.2. The Evolution of the O_2/CO Ratio

Even though molecular oxygen has yet to be observed in the local universe, O_2 may be more abundant at early cosmological epochs. At early times when O/C$\gg 1$, large quantities of O_2 could be produced simply because of an overabundance of oxygen relative to all of its antagonist species. In Figures 11 & 12 we plot the expected O_2/CO ratios in dark clouds as a function of the age and metallicity for the steady–state chemistry models. In general, the evolution of the O_2/CO ratio is most sensitive to the IMF and star formation efficiency and is not as dependent on n and τ_f. Basically, all models indicate that $O_2/CO \gtrsim 3$ within dark molecular clouds at early epochs. The models based on the stellar yields of M92 predict a rapid decrease of the O_2/CO ratio when $Z \rightarrow Z_\odot$ due to the excess carbon production from the winds of massive stars. The models based on the stellar yields of WW95 predict a slower decrease of the O_2/CO ratio since these models neglect the contribution of carbon from the winds of massive stars. The model solutions in Figures 11 & 12 are only applicable for molecular regions which are sufficiently shielded. In order to estimate the global molecular abundances in galaxies associated with an ensemble of molecular clouds with various values of total extinction, we must correct for the effects of photodissociation.

4.2.1. Correction for Photodissociation

The rate of photodissociation depends on the ambient UV field, and hence the SFR, and on the amount of metals shielding the molecular gas. Since the photodissociation rates for O_2 are larger than the rates for CO (van Dishoeck 1988), CO could exist in diffuse molecular clouds, while O_2 would not. Therefore, the spatial extent of the O_2 regions are expected to be smaller than the CO emission regions. Similarly, the extent of the CO regions is expected to be smaller than that of the H_2 regions since the H_2 molecules are more strongly self–shielded (van Dishoeck & Black 1988; Maloney & Black 1988). Assuming spherical geometry, we divide the molecular clouds into 3 distinct regions: (1) the central regions containing O_2, CO, and H_2, (2) the intermediate regions containing CO and H_2, and (3) the outer regions which contain only H_2. The relative extent of these regions depends on the radiation field and metallicity (i.e., the amount of dust). Maloney & Black (1988) have shown that near the edge of the CO regions, the amount of carbon contained within CO is strongly nonlinear with metallicity. For an average Galactic UV field (e.g., Draine 1978), we expect these edge effects to be important for cloud depths of $0 < A_V < 1.5$ (van Dishoeck & Black 1988). In deeper regions with extinctions larger than this critical value of $A_{CO} = 1.5$, the gas is sufficiently shielded so that virtually all of the carbon is contained within CO. By using the results of BLG95, we adopt a critical extinction value for O_2 of $A_{O_2} = 5$. Therefore, the molecular chemistry solutions of the O_2/CO ratios previously presented as Figures 11 & 12 are only valid for dark clouds with $A_V \gtrsim 5$.

The critical extinction boundaries of the CO and O_2 molecular regions depend on the ambient UV field. The aforementioned values of $A_{CO} = 1.5$ and $A_{O_2} = 5$ are for an average Galactic UV

field. In regions with more intense UV fields, the critical extinction values will be significantly larger. Using the study of photodissociation regions by Hollenbach, Takahshi, & Tielens (1991), we estimate that $A_{\rm CO} \propto G_o^{0.1}$, where G_o is the UV field relative to the solar neighborhood. Assuming that G_o is proportional to the SFR and that a similar relationship exists for both the CO and O_2 molecules, we expect that the critical extinction values for CO and O_2 should vary roughly as

$$A_{\rm CO} = 1.5 \left(\frac{SFR}{5\,M_\odot\,{\rm yr}^{-1}} \right)^{0.1}, \tag{19}$$

and

$$A_{\rm O_2} = 5.0 \left(\frac{SFR}{5\,M_\odot\,{\rm yr}^{-1}} \right)^{0.1}. \tag{20}$$

In equations (19&20) we use a Galactic SFR of $5\,M_\odot\,{\rm yr}^{-1}$ to normalize the critical extinction values for the average Galactic UV field.

In order to correct the global O_2/CO ratio for these photodissociation effects, we must estimate the mass fraction of the molecular gas contained within the O_2 and CO emission regions. Most of the molecular mass of galaxies is contained within giant molecular clouds (GMCs). We adopt a GMC mass distribution function of $dN/dM \propto M^{-3/2}$ with a lower mass limit of $10^4\,M_\odot$ and an upper limit of $2 \times 10^6\,M_\odot$ (Solomon & Rivolo 1987). Assuming a uniform density and using the size density relationship found for GMCs by Sanders, Scoville, & Solomon (1985), we find that the total extinction for a cloud at solar metallicity ($A_\odot$) and with a mass M in solar units is

$$A_\odot = 15(M/5.8 \times 10^5\,M_\odot)^{1/9}, \tag{21}$$

where a $5.8 \times 10^5\,M_\odot$ GMC (including a factor of 1.36 for helium) has a total H_2 column density of $N(H_2) = 1.5 \times 10^{22}\,{\rm cm}^{-2}$.

Assuming spherical geometry and integrating over an entire GMC of mass M, the total volume–weighted fraction of the H_2 mass coexisting with molecule x is

$$\frac{M({\rm H_2})^x}{M({\rm H_2})} = 3/R^3 \int_0^R \chi_x(r) r^2 dr, \tag{22}$$

where χ_x is the abundance of species x relative to its dark cloud abundance and R is the radius of the molecular cloud. Upon a change of variable $\tau/A_{total} = 1 - r/R$, the depth–dependence can be calculated as a function of the extinction τ. The total extinction of a cloud (A_{total}) varies linearly with the average density of dust particles (Spitzer 1978), which is expected to vary linearly with metallicity (Issa, MacLaren, & Wolfendale 1990; van den Hoek & de Jong 1992). We adopt $A_{total} = (Z/Z_\odot)A_\odot$, where $A_\odot$ is calculated from equation (21). Using the study of Maloney & Black (1988) to determine the CO abundance for low extinction regions near the edges of molecular clouds, we estimate that

$$\chi_x = \begin{cases} (\tau/A_x)^3 & \tau < A_x \\ 1 & \tau \geq A_x, \end{cases} \tag{23}$$

where A_x represent the critical extinction values of A_{CO} and A_{O_2} given by equations (19 &20). For metallicities less than $(A_{CO}/A_\odot)Z_\odot$, the total extinction of a GMC will be less than the critical extinction value for CO. In this case, the fractional mass of the CO regions is determined by the photodissociation edge–effects. Likewise, for metallicities less than $(A_{O_2}/A_\odot)Z_\odot$, the total extinction of the GMCs will be less than the critical extinction value for O_2, and the mass of the O_2 regions is dominated by the edge–effects. The total correction for photodissociation is calculated by summing over the GMC distribution function:

$$\frac{M(H_2)^{CO}}{M(H_2)} = \sum_{i=1}^{n} f_i \left(\frac{M(H_2)^{CO}}{M(H_2)} \right)_i , \tag{24}$$

and

$$\frac{M(H_2)^{O_2}}{M(H_2)} = \sum_{i=1}^{n} f_i \left(\frac{M(H_2)^{O_2}}{M(H_2)} \right)_i , \tag{25}$$

where f_i are the weighting coefficients normalized to unity. The $M(H_2)^{CO}/M(H_2)$ ratio is the fraction of the H_2 mass coexisting with CO, and $M(H_2)^{O_2}/M(H_2)$ is the fraction of the H_2 mass coexisting with O_2.

4.2.2. Other Scenarios Besides Steady State

Given the possible limitations of the steady–state solutions (§4.1), we analyze 2 additional scenarios for the evolution of the O_2/CO ratio: (1) the early–time scenario where the clouds do not reach their steady–state solutions and (2) the selective depletion of oxygen model. The early–time model solutions are presented in Figure 10. For O/C$\leq$ 10.1, the formal fit of the early–time scenario is given by

$$\log\left(\frac{O_2}{CO}\right) = -0.734 + 1.378 \log\left(\frac{O}{C}\right) - 6.740 \left(\frac{C}{O}\right)^2 . \tag{26}$$

For O/C $>$ 10.1, we assume that the early–time solutions are equivalent to those of steady state (eq. [18]).

In the scenario of selective oxygen depletion, the gas–phase $(C/O)_g$ ratio is enhanced relative to the total elemental C/O ratio. Since the proposed enhancement mechanisms of $(C/O)_g$ are primarily associated with grain processes, these effects are not expected to be as important at early cosmological epochs when the metallicity and dust abundances are lower on average. Studies of the nearby galaxies indicate that the dust–to–gas ratio is approximately proportional to the average metallicity (Issa et al. 1990; van den Hoek & de Jong 1992). Assuming a linear correlation with metallicity, we let γ be a free parameter describing the enhancement of C/O ratio, so that

$$(C/O)_g = [\gamma(Z/Z_\odot) + 1](C/O). \tag{27}$$

For the solar abundance ratio of C/O$\simeq$ 0.4, the observational limit for the O_2/CO ratio found by C91 would suggest that $\gamma \gtrsim 2$. We adopt this limiting case ($\gamma = 2$) for the selective depletion

of oxygen scenario. The dark cloud O_2/CO ratio in this model is determined by substituting the $(C/O)_g$ ratio given by equation (27) into equation (18).

For the three scenarios of (a) steady state, (b) early times, and (c) selective oxygen depletion, we use equations (24 &25) to determine the global volume–weighted O_2/CO abundance ratio corrected for photodissociation effects as a function of metallicity and the SFR. The global abundances are calculated using

$$\left(\frac{O_2}{CO}\right)_{global} = \left(\frac{M(H_2)^{O_2}}{M(H_2)^{CO}}\right)\left(\frac{O_2}{CO}\right)_{dark}, \tag{28}$$

where $(O_2/CO)_{dark}$ is the O_2/CO abundance ratio computed for the dark cloud solutions. In Figure 13 we show the evolution of the O_2/CO ratio for these scenarios compared with the dark cloud steady–state solutions. We choose 4 different models (Run 1, 10, 13, & 22) to represent examples of the closed box and infall models for both the M92 and WW95 stellar yields. The volume–weighted correction for photodissociation reduces the global O_2/CO ratios by a factor of approximately 30 at low metallicities. These corrections are fairly uncertain for low metallicities and greatly depend on the adopted parameterization describing the edge–effects (eq. [23]) and on the structure of the clouds. At solar metallicities using the stellar yields of WW95, only scenario (c) is consistent with the Galactic observational upper limit of the O_2/CO ratio. For the M92 models, all 3 scenarios are roughly consistent with the observational limits due to the higher carbon yields from stellar winds at solar metallicity. Interestingly, both the scenarios (b) & (c) for the M92 models predict a similar evolution of the O_2/CO ratio.

4.3. The Evolution of the CO, O_2, and Dust Abundances

The curves presented in Figures 11, 12 & 13 show the evolution of the O_2/CO ratio, but they do not indicate how much molecular gas is present. In order to determine the individual CO and O_2 abundances, we must first estimate several important parameters which are currently not known very well as a function of evolution and metallicity. These parameters include the molecular to neutral gas fraction $[M(H_2)/M(HI)]$ and the CO abundance relative to H_2. The determination of these factors is complicated by uncertainties in the empirical relation used to determine $M(H_2)$ from the observed CO luminosity. The first step in analyzing these complications and estimating the individual abundances of CO and O_2 is to estimate the molecular gas fraction.

The molecular gas fraction is uncertain for young galactic systems. The recent CO detections at high redshift are promising and indicate that at least some young galactic systems contain significant quantities of molecular gas (Brown & Vanden Bout 1991; Solomon et al. (1992); Barvainis et al. 1994a; Ohta et al. 1996; Omont et al. 1996b). Although optical absorption line studies along absorbing columns through damped Lyα systems suggest low molecular hydrogen abundances (Levshakov et al. 1992 and references therein; Ge & Bechtold 1997), these optical absorption line studies are strongly biased against detecting QSOs behind large columns of dust

(Fall & Pei 1995; Boissé 1995). Therefore, the global molecular masses associated with these young systems may be much larger than what would be inferred by only the optical observations. The global H_2/HI mass ratio is an important parameter for the models presented in this paper. Radio wavelength CO and HI emission line studies, in principle, can directly determine this mass ratio. Unfortunately, the 21–cm HI emission line, from which the HI mass is derived, is generally too weak to be observed at high redshift, and these observations are also often plagued by radio frequency interference. Since the global H_2/HI mass ratio has yet to be measured for any high redshift system, we apply the results determined from the studies of nearby galaxies.

In a compilation of low redshift CO data, Young & Scoville (1991) find that galaxies with early morphological types (S0–Sa) have molecular to neutral hydrogen mass ratios of $M(H_2)/M(HI) = 4.0 \pm 1.9$, whereas late–type galaxies (Sd–Sm) have ratios of $M(H_2)/M(HI) = 0.2 \pm 0.1$. Whether this result is a true representation of the molecular gas content as a function of morphological type is unclear. It is possible that these results reflect differences in the CO to H_2 conversion factor (Roberts & Haynes 1994). Young & Scoville (1991) assume a constant $M(H_2)/L(CO)$ ratio determined empirically from the study of Galactic clouds. This relation may underestimate the true amount of molecular gas in late–type galaxies which have lower average metallicities.

Recent observations indicate that the Galactic $M(H_2)$ to $L(CO)$ conversion factor does underestimate the molecular gas mass in metal–poor dwarf galaxies (Wilson 1995; Arimoto et al. 1996). The metallicity dependency implied by these observations suggests that $M(H_2)/L(CO) \propto (Z/Z_\odot)^{-0.7}$. This relationship is calibrated assuming that the total virial mass of $M(H_2)$ is given by the width of the CO line. Since the CO observations only measure the mass within the CO emission regions [$M(H_2)^{CO}$], not the potentially large envelopes of H_2 which contain no CO, we divide the molecular hydrogen gas into regions which contain CO and regions of lower extinction which do not have CO (§4.2). Assuming that 25% of the total gaseous mass is He, we find that

$$0.75M_g = M(H_2)^* + M(H_2)^{CO} + M(HI), \tag{29}$$

where $M(H_2)^*$ is the mass of H_2 in the regions without CO and $M(H_2)^{CO}$ is the mass of H_2 coexisting with the CO. We neglect the dust mass in equation (29) since the gas–to–dust mass ratios are typically of order 100 or larger. Solving for the total mass of CO molecules, we find that

$$M_{CO}(t) = 10.5[M(H_2)/M(H_2)^{CO} + M(HI)/M(H_2)^{CO}]^{-1} M_g(t)\xi_{CO}(t), \tag{30}$$

where ξ_{CO} is abundance of CO relative to H_2 within the CO emission regions. The $M(H_2)/M(H_2)^{CO}$ ratio is given by equation (24). By using the CO data for galaxies of different morphologies (Young & Knezek 1989) and the average metallicities as a function of morphological type (Roberts & Haynes 1994), we find an approximate relationship of $M(H_2)^{CO}/M(HI) \sim (Z/Z_\odot)$ assuming the Galactic $L(CO)$ to $M(H_2)^{CO}$ conversion factor. After correcting the conversion factor using the metallicity relationship found by Wilson (1995) and Arimoto et al. (1996), we find that $M(H_2)^{CO}/M(HI)$ is approximately constant; $M(H_2)^{CO}/M(HI) \sim 2$. We adopt this value for

equation (30).

The models of MH90 suggest that the CO abundance relative to H_2 within the CO emission regions scales directly with the elemental carbon abundance and is independent of the oxygen abundance as long as O/C> 1. For O/C< 1, most of the oxygen is tied up in CO, and $\xi_{\rm CO}$ is expected to scale with the oxygen abundance. By using the results of the MH90 models and normalizing the data to the Galactic CO abundance of $\xi_{\rm CO} = 10^{-4}$ (e.g., Young 1990), we adopt

$$\xi_{\rm CO} = \begin{cases} (Xc/Xc_{\odot})10^{-4} & {\rm O/C} \geq 1 \\ (Xo/Xo_{(o/c=1)})(Xc_{(o/c=1)}/Xc_{\odot})10^{-4} & {\rm O/C} < 1, \end{cases} \tag{31}$$

where Xc and Xo are the carbon and oxygen mass fractions calculated in the models of §2. The solar carbon mass fraction is $Xc_{\odot} = 0.00303$ (Grevesse & Anders 1989), and $Xc_{(o/c=1)}$ and $Xo_{(o/c=1)}$ are the carbon and oxygen mass fractions when O/C= 1.

After calculating the CO mass using equation (30), we compute the mass in molecular oxygen using

$$M_{\rm O_2}(t) = \frac{8}{7}\left[\frac{\rm O_2}{\rm CO}(t)\right] M_{\rm CO}(t), \tag{32}$$

where O_2/CO is derived for the different scenarios described in §4.2.

We calculate the dust mass in a straightforward fashion. We assume that the dust–to–gas ratio varies linearly with the average metallicity (Issa et al. 1990; van den Hoek & de Jong 1992), and we adopt the Galactic gas–to–dust ratio of $M_g/M_{dust} \sim 100$ (Savage & Mathis 1979; Mathis 1990; Tielens et al. 1996) to normalize the relationship;

$$M_{dust}(t) = 0.01(Z(t)/Z_{\odot})M_g(t), \tag{33}$$

where $M_g/M_{dust} = 100$ for solar metallicity. Uncertainties in the derived gas–to–dust ratios depend significantly on the composition of the grains which can have different frequency–dependent absorption coefficients that depend on temperature (e.g., Agladze et al. 1996). For the nearby IRAS galaxies, the derived gas to warm dust ratios are about a factor of 10 larger than the Galactic value, suggesting that most of the dust in galaxies is colder than 30 K (Devereux & Young 1990; Sanders, Scoville, & Soifer 1991). Even though more research into the properties of dust grains and sensitive observations at $\lambda > 100\mu$m are required to constrain the amount of cold dust in galaxies, equation (33) is currently an adequate approximation.

In Figures 14&15, we plot the evolution of the mass of CO, O_2, and dust as a function of metallicity and the gas fraction. The molecular masses fall off rapidly with decreasing metallicity due to the lack of shielding, while the dust masses decrease linearly with decreasing metallicity (Fig. 14) . We expect the largest O_2 masses in the metallicity range of $0.1 < Z/Z_{\odot} < 1$. Within this range of metallicities, there is enough dust to provide adequate shielding of the O_2 molecules, but the metallicity is low enough for high O/C ratios. For the models consistent with Galactic observations, the maximum of the O_2 mass occurs at early epochs ($\mu \gtrsim 0.5$, $z > 2$). The maximum

dust mass occurs later ($\mu \sim 0.4$) and is followed in time by the maximum CO mass (Fig. 15). This evolutionary progression is expected since the production of CO lags slightly behind the dust due to the increase of shielding with metallicity, while the O_2 abundances are largest at the lower metallicities when O/C$\gg 1$. By comparing the different models, we find several general results. Since the carbon stellar yields are smaller in the WW95 models, the $M(O_2)/M(\mathrm{CO})$ ratios for the WW95 models are larger than those for the M92 models. The dust masses in the M92 models are larger than the dust masses in the WW95 models, and these discrepancies are consistent with the differences between their effective net yields (Table 3). The situation is more subtle for the CO mass. As with $M(dust)$, the CO masses are larger in the M92 models. However, because the maximum M(CO) value occurs at a larger metallicity in the M92 models, the ratios of the M(CO) values (eq. [30 & 31]) between the M92 and WW95 models are larger than the ratios of their effective net yields.

For the Galactic disk, which has a total mass of $6 \times 10^{10}\, M_\odot$ (Bahcall & Soneira 1980) and an approximate H_2 mass of $M(H_2)^{\mathrm{CO}} \sim 2 \times 10^9$ (Solomon & Rivolo 1987), we estimate $M_{\mathrm{CO}}/M_T \sim 10^{-4}$ and $M_{dust}/M_T \sim 10^{-3}$ assuming $\mu = 0.1$ (Rana & Basu 1992). Depending on the details of the models, the total CO and dust masses for the Galactic disk inferred at earlier epochs are $\sim 2-5$ times larger than the current values. If we consider that some fraction of the Galactic halo mass ($\sim 2 \times 10^{12}\, M_\odot$, Peebles 1995) is baryonic, such as low mass stars and stellar remnants, the mass of CO and dust for the entire Galaxy may have been more than an order of magnitude larger at the earlier epochs.

5. Observational Studies

In the previous section, we have calculated the evolution of the abundance of CO, O_2, and dust in galaxies. In this section we discuss the feasibility of observing these species in galaxies at high redshift.

5.1. Observations of Dust at High Redshift

Several researchers have already addressed the favorable prospects for observations of dust at high redshift (Braine 1995; Eales & Edmunds 1996), and many detections of dust in high redshift radio galaxies and quasars have recently been reported (McMahon et al. 1994; Chini & Krügel 1994; Dunlop et al. 1994; Isaak et al. 1994; Ivison 1995; Omont et al. 1996a). For a universe with $q_o \sim 0.5$ and $z > 1$, intrinsically similar sources observed at mm or sub–mm wavelengths have observed flux densities which actually increase with increasing redshift, due to the strong dependency of the dust emission on the rest–frame frequency (McMahon et al. 1994). Including the effects of chemical evolution, we expect even brighter observed flux densities because of the larger dust masses at earlier epochs (§4.3). To quantify this statement, we calculate the observed

flux density $S_{\nu_{obs}}$ implied by the dust mass using the expressions given by McMahon et al. (1994):

$$M_{dust} = S_{\nu_{obs}} D_L^2 [(1+z)\kappa_d(\nu_r) B(\nu_r, T_d)]^{-1}, \tag{34}$$

where D_L is the luminosity distance which is given by

$$D_L = c H_o^{-1} q_o^{-2} (q_o z + (q_o - 1)[(1 + 2q_o z)^{1/2} - 1]), \tag{35}$$

and $B(\nu_r, T_d)$ is the Planck blackbody function for a rest–frame frequency ν_r and dust temperature T_d. For the absorption coefficient of dust κ_d, we use a simple power law (Downes et al. 1992):

$$\kappa_d = \begin{cases} 0.4(\nu_r/250\,\mathrm{GHz})^2\,\mathrm{cm}^2\,\mathrm{g}^{-1} & \nu_r < 1200\,\mathrm{GHz} \\ 1.92(\nu_r/250\,\mathrm{GHz})\,\mathrm{cm}^2\,\mathrm{g}^{-1} & \nu_r > 1200\,\mathrm{GHz}. \end{cases} \tag{36}$$

The dust absorption coefficient is uncertain, but it is expected to increase with ν^1 at the short infrared wavelengths and vary with ν^2 at longer wavelengths (Schwartz 1982; Hildebrand 1983).

In Figure 16 we show the evolution of the calculated thermal dust flux density observed at 240 GHz (1.25 mm) as a function of redshift. The models in Figure 16 are for galaxies with a total final baryonic mass of $10^{12}\,M_\odot$. By including evolution, the computed flux densities are increased significantly with respect to the nonevolutionary models. For the closed box models, the maximum intensity occurs before the maximum dust mass due to the increasing flux density with increasing rest–frame frequency at high redshift (for $q_o \sim 0.5$). These effects are less important for the infall models since the maximum amount of gaseous metals occurs at later epochs. The results presented in this paper suggest that observations of dust emission from high–redshift young galaxies at mm and sub–mm wavelengths are feasible. Both the IRAM 30 m telescope bolometer system (Wild 1995) and the Submillimeter Common User Bolometer Array [SCUBA] on the James Clerk Maxwell Telescope (Matthews 1996) have sensitivities of approximately 1–2 mJy for several hours of integration which is sufficient to detect gas–rich galaxies with total masses of $M \gtrsim few \times 10^{11}\,M_\odot$ at high redshift. The next generation of mm–wavelength synthesis telescopes will achieve far greater sensitivities of 0.1–0.2 mJy in only a minute of integration (Brown 1997) and will be very suitable for this research.

5.2. Observations of Molecular Gas at High Redshift

Despite many searches for CO emission in several different types of suspected young galaxies, including QSOs, high redshift radio galaxies, and damped Lyα systems (Wiklind & Combes 1994; van Ojik 1995; Barvainis & Antonucci 1996; Ivison et al. 1996; Frayer 1996; Evans et al. 1996; Yun & Scoville 1997), the list of CO sources at high redshift is still very limited. Currently, the only three confirmed CO emission detections at high redshift are for IRAS F10214+4724 (Brown & Vanden Bout 1991; Solomon et al. 1992), the Cloverleaf quasar (Barvainis et al. 1994a), and the quasar BR1202-0725 (Ohta et al. 1996; Omont et al. 1996b). These systems have

molecular masses of approximately $10^{11}\,M_{\odot}$, assuming the Galactic CO–to–H_2 conversion factor and assuming no gravitational amplification. Both the Cloverleaf quasar (Kayser et al. 1990) and IRAS F10214+4724 are lensed systems (Graham & Liu 1995; Broadhurst & Lehar 1995). It is still not known if lensing is important for BR1202-0725. Regardless of the precise interpretation of these high–redshift systems, the observations indicate that these systems have CO luminosities comparable to the most luminous infrared galaxies seen at the current epoch (Downes, Solomon, & Radford 1993; Barvainis et al. 1995) and that copious amounts of metals were produced very early in the history of the Universe ($t \lesssim 1$ Gyr).

One of the goals of the models presented in this paper is to determine the possibility of observing molecular oxygen during the early stages of galaxy evolution. Unlike CO, molecular oxygen is optically thin under most ISM conditions (Black & Smith 1985). For the ground state transition of $^{16}O_2[N(J) = 1(1) \rightarrow 1(0)]$ which has a rest frequency of 118.75 GHz, the line intensity in $\mathrm{K\,km\ s^{-1}}$ is given by

$$I(\mathrm{O_2}) = 6.8 \times 10^{-16} N(\mathrm{O_2})/T, \tag{37}$$

where $N(O_2)$ is the column density in $\mathrm{cm^{-2}}$ and T is the excitation temperature of the gas in Kelvin (L92). The intensity of the ground state O_2 transition relative to the CO(1→0) line is given by

$$\frac{I(\mathrm{O_2})}{I(\mathrm{CO})} = 0.68 \left(\frac{N(\mathrm{O_2})}{N(\mathrm{CO})}\right) \left(\frac{\alpha_{\mathrm{CO}}}{\alpha_{\mathrm{CO,G}}}\right) \left(\frac{\xi_{\mathrm{CO}}}{10^{-4}}\right) \left(\frac{30\,\mathrm{K}}{T}\right), \tag{38}$$

where $\alpha_{\mathrm{CO,G}}$ is the Galactic CO–to–H_2 conversion factor (e.g., Scoville & Sanders 1987). The global–averaged column density ratio $N(O_2)/N(CO)$ corrected for relative filling factors is

$$\frac{N(\mathrm{O_2})}{N(\mathrm{CO})} = \left(\frac{\mathrm{O_2}}{\mathrm{CO}}\right)_{dark} \times \left(\frac{M(\mathrm{H_2})^{\mathrm{O_2}}}{M(\mathrm{H_2})^{\mathrm{CO}}}\right)^{2/3}, \tag{39}$$

where $(O_2/CO)_{\mathrm{dark}}$ is the abundance ratio within the dark clouds and the ratio $M(H_2)^{O_2}/M(H_2)^{CO}$ is the volume–weighted mass fractions given by equations (24&25).

An implicit assumption within equation (38) is that both the O_2 and CO lines are probing optically thick dense molecular clouds. For very powerful starbursts, the CO line emission may arise predominantly from diffuse regions of low CO–optical depths near the surfaces of molecular clouds (Aalto et al. 1995), while the O_2 lines would probe only the dark cloud cores. In such a scenario, the O_2/CO line ratio would have little relationship to the actual global O_2/CO abundance ratio. However, it is still unclear if the ^{12}CO emission from starburst galaxies is actually dominated by regions of low optical depth. For the nearby starburst galaxy M82, Wild et al. (1992) find that the ^{12}CO emission arises from the optically thick dense clouds, and in this case equation (38) would be applicable after correcting for the relative CO and O_2 filling factors (eq.[39]). In addition, we expect the CO emission to arise mainly from the cloud cores in metal–poor starbursts due to the lack of shielding in the diffuse regions.

The Galactic CO–to–H_2 conversion factor is expected to vary with metallicity in low metallicity systems, and at metallicities above solar the conversion factor is expected to be

constant since the CO emission becomes optically thick and thermalized (Maloney 1990; Sakamoto 1996). Using these assumptions, we adopt the following expression:

$$\left(\frac{\alpha_{\rm CO}}{\alpha_{\rm CO,G}}\right) = \begin{cases} (Z/Z_\odot)^{-0.7} & Z < Z_\odot \\ 1 & Z \geq Z_\odot, \end{cases} \tag{40}$$

where the power–law index of -0.7 has been observationally estimated (Wilson 1995). We emphasize that equation (40) has been determined using a relatively small sample of low metallicity galaxies. Significant deviations may exist from galaxy to galaxy or within any particular galaxy. For example, observations of clouds in the LMC and SMC indicate a similar range of CO–to–H_2 conversion factors despite their different metallicities (Rubio 1997). These results suggest that the conversion factor is not solely based on metallicity (e.g., see appendix in Bryant & Scoville 1996).

The mass of the H_2 molecules within the CO emission regions in $M_\odot$ is related to the CO line intensity $I({\rm CO})$ by

$$M({\rm H_2})^{\rm CO} h^2 = 1.0 \times 10^{12} \left(\frac{\alpha_{\rm CO}}{\alpha_{\rm CO,G}}\right) 1.06 \left(\frac{I_{\rm CO}}{\rm mJy}\right) \left(\frac{\Delta V}{\rm km\ s^{-1}}\right) \frac{q_o^{-4} Q^2}{\nu_{rest}^2 (1+z)}, \tag{41}$$

where ν_{rest} is the rest frequency of the CO transition in GHz [$\nu_{rest} = 115.27$ for the CO(1→0) line] and Q is a term associated with the luminosity distance; $Q = q_o z + (q_o - 1)[(1 + 2q_o z)^{1/2} - 1]$. The factor of 1.06 arises from assuming a Gaussian line shape with a FWHM line width of ΔV.

In §4.3 we have calculated $M({\rm H_2})^{\rm CO}$. Using equation (41), we calculate $I({\rm CO})$, and then we determine $I({\rm O_2})$ from equation (38), assuming $T = 30\,{\rm K}$. For these calculations, we adopt a FWHM line width of $300\,{\rm km\ s^{-1}}$, which is approximate CO line widths for the previous high–redshift CO detections. We show the results of the computed evolution of the CO(1→0) and $O_2(1,1 \rightarrow 1,0)$ line intensities for a variety of models in Figure 17. These intensities may be scaled linearly with the final total baryonic mass in units of $10^{12}\,M_\odot$, and the curves scale inversely with line width. The nonevolutionary solutions assume a constant $M({\rm CO})$ value which is the mass that is reached in the numerical models at $t = 10$ Gyr.

Currently, only the most massive or lensed galaxies can be detected in CO emission. With the next generation of radio telescopes, such as the NRAO Green Bank Telescope (GBT), the Large Millimeter Telescope (LMT), and the proposed mm–wavelength synthesis telescopes, redshifted CO detections should be commonplace. With several hours of integration using these new instruments, we should be able to detect high–redshift CO line strengths of $\sim 0.1 - 0.5\,{\rm mJy}$ (Brown 1997). This sensitivity is sufficient to detect the CO(1→0) line in young massive galaxies (Fig. 17). Due to the ν_{rest}^2 term in equation (41), observations of the higher transitions of CO ($J_{upper} > 1$) can provide even more sensitive measurements of the molecular gas mass, as long as the brightness temperature and the size of the source do not decrease substantially compared to the CO(1→0) source (Solomon et al. 1992). Since starbursting galaxies at the current epoch have similar brightness temperatures for the CO(1→0) and CO(3→2) lines (Devereux et al. 1994)

and given that the CO(6→5) and CO(7→6) lines have already been detected at high–redshift, we expect equation (41) to be valid for at least the moderately high CO transitions, such as CO(3→2) and CO(4→3), in high–redshift starburst galaxies. If this assumption is correct, the CO(3→2) and CO(4→3) line intensities could be estimated by multiplying the CO(1→0) curves in Figure 17 by factors of 9 and 16, respectively. Even with the new instruments and observations of the moderately high CO transitions, the Milky Way ($M_T \sim 10^{11}\, M_\odot$) placed at high redshifts would still be very difficult to detect, assuming no evolution. However, the gas–rich predecessors of galaxies similar to the Milky Way are expected to be observable.

The calculations presented in this paper suggest that both dust emission and CO line emission will be readily observable at high redshift with the next generation mm and sub–mm wavelength telescopes. Observations of molecular oxygen will be significantly more difficult. We require sensitivities of order 0.01 mJy for the O_2 lines at high redshift to discriminate between the possible scenarios presented in this paper. However, the predicted O_2 intensities greatly depend on many uncertain parameters associated with photodissociation, molecular cloud chemistry, and the densities and structure of molecular clouds. For simplicity, we have assumed uniform GMC densities. If molecular clouds are comprised of high–density clumps at low metallicities (Lequeux et al. 1994), we may have underestimated the global O_2/CO mass ratios at early epochs. Given the theoretical uncertainties, observations of O_2 in high–redshift CO sources could still be fruitful. In addition to high–redshift systems, metal–poor galaxies at the current epoch may have enhanced O_2 abundances. Ground–based observations of metal–poor starbursts at $z \gtrsim 0.03$ and observations of the LMC and SMC with satellite telescopes, such as ODIN (Hjalmarson 1997), could provide stringent constraints on the metallicity dependency of the O_2/CO ratio. Absorption line searches (e.g., Combes & Wiklind 1995) along known low metallicity lines–of–sights could even be more discriminating than the emission line studies. Furthermore, new O_2 excitation calculations suggest the possibility of O_2 maser emission for the N(J)=N(J)→N(J−1) transitions within dense clouds (Bergman 1995). Without question, observations are required to constrain the different theoretical hypotheses.

In this paper we have concentrated on the molecular lines. For the high rates of star formation expected in forming galaxies, the infrared atomic lines which probe the photodissociation regions (Watson 1985) may be significantly brighter than the molecular lines. The redshifted neutral atomic carbon transitions have been observed in both F10214+4724 (Brown & Vanden Bout 1992) and the Cloverleaf (Barvainis et al. 1994b). Searches for the redshifted C^+, N^+, and atomic oxygen lines, which should all be stronger than the neutral carbon lines, are becoming more feasible with instrumentation improvements. With observations of both the atomic lines and the molecular lines, we can constrain the H_2/H ratios at high redshift and gain insight into the strength of the photodissociation fields associated with young galaxies. If the majority of oxygen is not molecular, we would expect relatively strong atomic oxygen emission lines from protogalaxies, given the expected large O/C ratios at early epochs. Since there are currently only a few observations at high redshift, we cannot predict with any certainty which atomic or molecular emission lines will

be the strongest. Future observations will constrain the various possibilities.

6. Conclusions

By drawing upon the current knowledge in the fields of stellar evolution, galactic chemical evolution, and chemical processes within molecular clouds, we have constructed a general set of models to compute the evolution of the abundance of CO, O_2 and dust as a function of age and metallicity for massive galaxies. Over a wide range of input parameters, the models suggest the following general conclusions:

- The mass of gaseous metals (ZM_g) achieves its maximum at redshifts of $z \sim 1 - 3$ when the metallicity is approximately solar and when approximately 1/2 of the galaxy mass is in gas.
- The O/C ratio is expected to be $\gtrsim 10$ at early epochs.
- The observed increase in the C/O ratio with metallicity may suggest significant contributions to the yields from the winds of massive stars.
- The O_2/CO ratio is expected to be of order unity in dark clouds ($A_V \gtrsim 5$) during the early stages of galaxy evolution.
- At the low metallicities, the global O_2/CO abundance ratios corrected for photodissociation are are expected to be reduced by over an order of magnitude relative to the dark cloud solutions.
- The maximum CO and dust masses for young galaxies are expected to be at least 2–5 times larger than the values found for normal galaxies in the local universe.
- The largest O_2 masses are expected for chemically young systems with metallicities of $0.1 < Z/Z_\odot < 1$ and large gas fractions ($\mu \gtrsim 0.5$).
- The models suggest that thermal dust emission and CO line emission should be observable for young massive galaxies at high redshift, and that even O_2 emission may be observable in chemically young galaxies.
- The largest uncertainties in the models presented here are associated with the O_2 abundances. The existence of detectable quantities of O_2 greatly depends on how metallicity, photodissociation, turbulent mixing, and grain processes affect the molecular gas–phase abundances.

In summary, all models predict more gaseous metals for young galaxies since the mass of gaseous metals has been depleted in galaxies at the current epoch due to star formation. The models also indicate that the abundances of the oxygen species, such as O_2, should be enhanced

at earlier epochs. The models presented in this paper depend on many uncertain parameters and approximations which require further investigation. Future observations of dust, CO, O_2, and the atomic species will constrain the theoretical models and will greatly enhance our knowledge of protogalaxies.

We thank S. Woosley and T. Weaver for their tables of supernova ejecta. We thank A. Maeder for communications concerning the yields in M92. We are also very grateful to J. Black for several helpful comments and suggestions. DTF was supported by the NRAO predoctoral program and by a postdoctoral fellowship funded by the University of Toronto.

REFERENCES

Aalto, S., Booth, R. S., Black, J. H., & Johansson, L. E. B. 1995, A&A, 300, 369

Agladze, N. I., Sievers, A. J., Jones, S. A., Burlitch, J. M., & Beckwith, S. V. W. 1996, ApJ, 462, 1026

Arimoto, N., Sofue, Y., & Tsujimoto, T. 1996, PASJ, 48, 275

Bahcall, J. N., & Soneira, R. M. 1980, ApJS, 44, 73

Bally, J., Shull, J. M., & Hamilton, A. J. S. 1993, in The Evolution of Galaxies and Their Environment, ed. D. Hollenbach, H. Thronson, & J. M. Shull (NASA Conference Pub. 3190), 345

Barvainis, R., & Antonucci, R. 1996, PASP, 108, 187

Barvainis, R., Antonucci, R., Hurt, T., Coleman, P. & Reuter, H.-P. 1995, ApJ, 451, L9

Barvainis, R., Tacconi, L., Antonucci, R., Alloin, D., & Coleman, P. 1994a, Nature, 371, 586

Barvainis, R., Tacconi, L., Antonucci, R., Alloin, D., Coleman, P., & Maloney, P. 1994b, BAAS, 26, 1340

Bergin, E. A., Langer, W. D., & Goldsmith, P. F. 1995 (BLG95), ApJ, 441, 222

Bergman, P. 1995, ApJ, 445, L167

Black, J. H., & Smith, P. L. 1985, ApJ, 277, 562

Blake, G. A., Sutton, E. C., Masson, C. R., & Phillips, T. G. 1987, ApJ, 315, 621

Boissé, P. 1995, in QSO Absorption Lines, ed., G. Meylan (Berlin: Springer–Verlag), 35

Braine, J. 1995, A&A, 300, 687

Broadhurst, T., & Lehar, J. 1995, ApJ, 450, L41

Brown, R. L. 1997, in CO: Twenty–five Years of Millimeter–wave Spectroscopy, ed. W. B. Latter et al. (Dordrecht: Kluwer), 247

Brown, R. L., & Vanden Bout, P. A. 1991, AJ, 102, 1956

Brown, R. L., & Vanden Bout, P. A. 1992, ApJ, 397, L11

Bryant, P. M., & Scoville, N. Z. 1996, ApJ, 457, 678

Burkert, A., Truran, J. W., & Hensler, G. 1992, ApJ, 391, 651

Cardelli, J. A., Mathis, J. S., Ebbets, D. C., & Savage, B. D. 1993 (C93), ApJ, 402, L17

Carigi, L. 1994, ApJ, 424, 181

Chieffi, A., Straniero, O., & Salaris, M. 1995, ApJ, 445, L39

Chièze, J. P., & Pineau des Forêts, G. 1989, A&A, 221, 89

Chini, R., & Krügel, E. 1994 A&A, 288, L33

Clayton, D. D. 1987, ApJ, 315, 451

Clegg, R. E. S., Lambert, D. L., & Tomkin, J. 1981, ApJ, 250, 262

Combes, F., Casoli, F., Encrenaz, P., Gerin, M., & Laurent, C. 1991 (C91), A&A, 248, 607

Combes, F., & Wiklind, T. 1995, A&A, 303, L61

Cunha, K., & Lambert, D. L. 1994, ApJ, 426, 170

de Graauw, Th. et al. 1996, A&A, 315, L345

Devereux, N., Taniguchi, Y., Sanders, D. B., Nakai, N., & Young, J. S. 1994, AJ, 107, 2006

Devereux, N. A., & Young, J. S. 1990, ApJ, 359, 42

d'Hendecourt, L. B., & Jourdain de Muizon, M. 1989, A&A, 223, L5

Dopita, M. A., & Ryder, S. D. 1994, ApJ, 430, 163

Downes, D., Radford, S. J. E., Greve, A., Thum, C., Solomon, P. M., & Wink, J. E. 1992, ApJ, 398, L25

Downes, D., Solomon, P. M., & Radford, S. J. E. 1993, 414, L13

Draine, B. T. 1978, ApJS, 36, 595

Dunlap, J. S., Hughes, D. H., Rawlings, S., Eales, S. A., & Ward, M. J. 1994, Nature, 370, 347

Eales, S., & Edmunds, M. G. 1996, MNRAS, 280, 1167

Edmunds, M. 1990, MNRAS, 246, 678

Ehrenfreund, P., Breukers, R., d'Hendecourt, L., & Greenberg, J. M. 1992, A&A, 260, 431

Evans, A. S., Sanders, D. B., Mazzarella, J. M., Solomon, P. M., Downes, D., Kramer, C., & Radford, S. J. E. 1996, ApJ, 457, 658

Fall, S. M., & Pei, Y. C. 1993, ApJ, 402, 479

Fall, S. M., & Pei, Y. C. 1995, in QSO Absorption Lines, ed., G. Meylan (Berlin: Springer–Verlag), 23

Frayer, D. T. 1996, Ph.D. Thesis, University of Virginia

Freedman, W. L., et al. 1994, Nature, 371, 757

Frerking, M. A., Langer, W. D., & Wilson, R. W. 1982, ApJ, 262, 590

Fritze–v. Alvensleben, U., Krüger, H., Fricke, K. J., & Loose, H.–H. 1989, A&A, 224, L1

Fuente, A., Cernicharo, J., García–Burillo, S., & Tejero, J. 1993, A&A, 275, 558

Garnett, D. R., Skillman, E. D., Dufour, R. J., Peimbert, M., Torres–Peimbert, S., Terlevich, R. J., Terlevich, E., & Shields, G. A. 1995, ApJ, 443, 64

Ge, J., & Bechtold, J. 1997, ApJ, 477, L73

Gensheimer, P. D., Mauersberger, R., & Wilson, T. L. 1996, A&A, 314, 281

Goldsmith, P. F., Snell, R. L., Erickson, N. R., Dickman, R. L., Schloerb, F. P., & Irvine, W. M. 1985, ApJ, 289, 613

Goldsmith, P. F., & Young, J. S. 1989 (GY89), ApJ, 341, 718

Graedel, T. E., Langer, W. D., & Frerking, M. A. 1982, ApJS, 48, 321

Graham, J. R., & Liu, M. C. 1995, ApJ, 449, L29

Grevesse, N., & Anders, E. 1989, in Cosmic Abundances of Matter, ed. J. Waddington (New York: American Institute of Physics), 1

Harrison, A., Brand, P., Russell, A., & Puxley, P. 1995, Ap&SS, 224, 473

Hasegawa, T. I., & Herbst, E. 1993, MNRAS, 261, 83

Herbst, E., & Leung, C. M. 1986 (HL86), ApJ, 310, 378

Herbst, E., & Leung, C. M. 1989 (HL89), ApJS, 69, 271

Hildebrand, R. H. 1983, QJRAS, 24 267

Hollenbach, D. J., Takahashi, T., & Tielens, A. G. G. M. 1991, ApJ, 377, 192

Hjalmarson, Å. 1997, in CO: Twenty–five Years of Millimeter–wave Spectroscopy, ed. W. B. Latter et al. (Dordrecht: Kluwer), 227

Hunter, D. A., & Gallagher, J. S. 1985, ApJS, 58, 533

Impey, C., & Bothun, G. 1989, ApJ, 341, 89

Isaak, K. G., McMahon, R. G., Hills, R. E., & Withington, S. 1994, MNRAS, 269, L28

Issa, M. R., MacLaren, I., & Wolfendale, A. W. 1990, A&A, 236, 237

Ivison, R. J. 1995, MNRAS, 275, L33

Ivison, R. J., Papadopoulos, P., Seaquist, E. R., & Eales, S. 1996, MNRAS, 278, 669

Kayser, R., Surdej, J., Condon, J. J., Kellermann, K. I., Magain, P., Remy, M., & Smette, A. 1990, ApJ, 364, 15

Kennicutt, R. C., Jr. 1989, ApJ, 344, 685

Kraemer, S. B., Wu, C.–C., Crenshaw, D. M., & Harrington, J. P. 1994 (K94), ApJ, 435, 171

Langer, W. D., & Graedel, T. E. 1989 (LG89), ApJS, 69, 241

Lanzetta, K. M., Wolfe, A. M., Turnshek, D. A., Lu, L., Hazard, C., & McMahon, R. G.1991, ApJS, 77, 1

Lanzetta, K. M., Wolfe, A. M., & Turnshek, D. A. 1995, ApJ, 440, 435

Larson, R. B. 1972, Nature Phys. Sci., 236, 7

Lequeux, J., Le Bourlot, J., Pineau des Forêts, G., Roueff, E., Boulanger, F., & Rubio, M. 1994, A&A 292, 371

Levshakov, S. A., Chaffee, F. H., Foltz, C. B., & Black, J. H. 1992, A&A, 262, 385

Liszt, H. S. 1985, ApJ, 298, 281

Liszt, H. S. 1992 (L92), ApJ, 386, 139

Liszt, H. S., & Vanden Bout, P. A. 1985 (LV85), ApJ, 291, 178

Maeder, A. 1992 (M92), A&A, 264, 105

Maloney, P. 1990, in The Interstellar Medium in Galaxies, ed. H. A. Thronson, Jr. & J. M. Shull (Dordrecht: Kluwer), 493

Maloney, P., & Black, J. H. 1988, ApJ, 325, 389

Maréchal, P., Pagani, L., Langer, W. D., & Castets, A. 1997, A&A, 318, 252

Mathis, J. S. 1990, ARA&A, 28, 37

Matteucci, F., & Chiosi, C. 1983, A&A, 123, 121

Matteucci, F., & Tornambè, A. 1987, A&A, 185, 51

Matthews, H. E. 1996, The James Clerk Maxwell Telescope: A Guide for the Prospective User

McMahon, R. G., Omont, A., Bergeron, J., Kreysa, E., & Haslam, C. G. T. 1994, MNRAS, 267, L9

Meyer, D. M., Jura, M., Hawkins, I., & Cardelli, J. A. 1994 (M94), ApJ, 437, L59

Mezger, P. G. 1987, in Starbursts and Galaxy Evolution, ed. T.X. Thuan, T. Montmerle, & J. Tran Thanh Van (Gif sur Yvette: Frontières), 3

Millar, T. J., & Herbst, E. 1990 (MH90), MNRAS, 242, 92

Ohta, K., Yamada, T., Nakanishi, K., Kohno, K., Akiyama, M., & Kawabe, R. 1996, Nature, 382, 426

Omont, A., McMahon, R. G., Cox, P., Kreysa, E., Bergeron, J., Pajot, F., & Storrie–Lombardi, L. J. 1996a, A&A, 315, 1

Omont, A., Petitjean, P., Guilloteau, S., McMahon, R. G., Solomon, P. M., & Pécontal, E. 1996b, Nature, 382, 428

Pagel, B. E. J. 1987, in The Galaxy, ed. G. Gilmore & B. Carswell (Dordrecht: Reidel), 341

Pagel, B. E. J., & Edmunds, M. G. 1981, ARA&A, 19, 77

Peebles, P. J. E. 1995, ApJ, 449, 52

Pei, Y. C., Fall, S. M., & Bechtold, J. 1991, ApJ, 378, 6

Petitjean, P., Rauch, M., & Carswell, R. F. 1994, A&A, 291, 29

Pettini, M., Smith, L. J., Hunstead, R. W., & King, D. L. 1994, ApJ, 426, 79

Pierce, M. J., Welch, D. L., McClure, R. D., van den Bergh, S., Racine, R., & Stetson, P. B. 1994, Nature, 371, 385

Pineau des Forêts, G., Flower, D. R., & Chièze, J.–P., 1992 (PFC92), MNRAS, 256, 247

Prantzos, N., Vangioni–Flam, E., & Chauveau, S. 1994, A&A, 285, 132

Prasad, S. S., & Huntress, W. T., Jr. 1980, ApJ, 239, 151

Press, W. H., Flannery, B. P., Teukolsky, S. A., & Vetterling, W. T. 1986, Numerical Recipes (Cambridge: Cambridge Univ. Press)

Rana, N. C. 1991, ARA&A, 29 129

Rana, N. C., & Basu, S. 1992, A&A, 265, 499

Renzini, A., & Voli, M. 1981 (RV81), A&A, 94, 175

Roberts, M. S., & Haynes, M. P. 1994, ARA&A, 32, 115

Rubio, M. 1997, in CO: Twenty–five Years of Millimeter–wave Spectroscopy, ed. W. B. Latter et al. (Dordrecht: Kluwer), 265

Sakamoto, S. 1996, ApJ, 462, 215

Salpeter, E. E. 1955, ApJ, 121, 161

Sandage, A. 1986, A&A, 161, 89

Sanders, D. B., Scoville, N. Z., & Soifer, B. T. 1991, ApJ, 370, 158

Sanders, D. B., Scoville, N. Z., & Solomon, P. M. 1985, ApJ, 289, 373

Savage, B. D., & Mathis, J. S. 1979, ARA&A, 17, 73

Schaller, G., Schaerer, D., Meynet, G., & Maeder,A. 1992, A&AS, 96, 269

Schilke, P., Carlstrom, J. E., Keene, J., & Phillips, T. G. 1993, ApJ, 417, L67

Schmidt, M. 1959, ApJ, 129, 243

Schneider, D. P., Schmidt, M., & Gunn, J. E. 1991, AJ, 102, 837

Schwartz, P. R. 1982, ApJ, 252, 589

Scoville, N. Z., & Sanders, D. B. 1987, in Interstellar Processes, ed. D. J. Hollenbach & H. A. Thronson, Jr. (Dordrecht: D. Reidel Pub. Co.), 21

Smith, R. G., Sellgren, K., & Brooke, T. Y. 1993, MNRAS, 263, 749

Solomon, P. M., Downes, D., & Radford, S. J. E. 1992, ApJ, 398, L29

Solomon, P. M., & Rivolo, A. R. 1987, in The Galaxy, ed. G. Gilmore & B. Carswell (Dordrecht: D. Reidel Pub. Co.), 105

Spitzer, L., Jr. 1978, Physical Processes in the Interstellar Medium (New York: John Wiley & Sons)

Steidel, C. C., Giavalisco, M., Pettini, M., Dickinson, M., & Adelberger, K. L. 1996, ApJ, 462, L17

Stutzki, J. et al. 1997, ApJ, 477, L33

Theis, Ch., Burkert, A., & Hensler, G. 1992, A&A, 265, 465

Tielens, A. G. G. M., Wooden, D. H., Allamandola, L. J., Bregman, J., & Witteborn, F. C. 1996, ApJ, 461, 210

Timmes, F. X., Woosley, S. E., & Weaver, T. A. 1995, ApJS, 98, 617

Tinsley, B. M. 1972, ApJ, 178, 319

Tinsley, B. M. 1980, Fundamentals of Cosmic Physics, 5, 287

Tomkin, J., Lemke, M., Lambert, D. L., & Sneden, C. 1992, AJ, 104, 1568

Turnshek, D. A., Kopko, M., Jr., Monier, E., Noll, D., Espey, B. R., & Weymann, R. J. 1996, ApJ, 463, 110

van den Hoek, B., & de Jong, T. 1992, in The Feedback of Chemical Evolution on the Stellar Content of Galaxies, ed. D. Alloin & G. Stasinska (Meudon: Pub. de l'Observatoire de Paris), 289

van Dishoeck, E. F. 1988, in Rate Coefficients in Astrochemistry, ed. T. J. Millar & D. A. Williams (Dordrecht: Kluwer), 49

van Dishoeck, E. F., & Black, J. H. 1988, ApJ, 334, 771

van Dishoeck, E. F., & Helmich, F. P. 1996, A&A, 315, L177

van Ojik, R. 1995, Ph.D. Thesis, University of Leiden

Watson, D. M. 1985, Physica Scripta, T11, 33

Whittet, D. C. B. 1993, in Dust and Chemistry in Astronomy, ed. T. J. Millar & D. A. Williams (Bristol: Institute of Physics Pub.), 9

Whittet, D. C. B., et al. 1996, A&A, 315, L357

Wiklind, T., & Combes, F. 1994, A&A, 288, L41

Wild, W. 1995, The 30m Manual: A Handbook for the IRAM 30m Telescope

Wild, W., Harris, A. I., Eckart, A., Genzel, R., Graf, U. U., Jackson, J. M., Russell, A. P. G., & Stutzki, J. 1992, A&A, 265, 447

Willacy, K., & Williams, D. A. 1993, MNRAS, 260, 635

Wilson, C. D. 1995, ApJ, 448, L97

Wolfe, A. M., Turnshek, D. A., Smith, H. E., & Cohen, R. D. 1986, ApJS, 61 249

Woosley, S. E., & Weaver, T. A. 1995 (WW95) ApJS, 101, 181

Xie, T., Allen, M., & Langer, W. D. 1995 (XAL95), ApJ, 440, 674

Young, J. S. 1990, in The Interstellar Medium in Galaxies, ed. H. A. Thronson, Jr. & J. M. Shull (Dordrecht: Kluwer), 67

Young, J. S., & Knezek, P. M. 1989, ApJ, 347, L55

Young, J. S., & Scoville, N. Z. 1991, ARA&A, 29, 581

Yun, M. S. & Scoville, N. Z. 1997, in CO: Twenty–five Years of Millimeter–wave Spectroscopy, ed. W. B. Latter et al. (Dordrecht: Kluwer), 341

Zmuidzinas, J., Blake, G. A., Carlstrom, J., Keene, J., Miller, D., & Schilke, P. 1996, ApJ, submitted

Fig. 1.— The stellar yields of oxygen (mp_O) and carbon (mp_C) calculated by Woosley & Weaver (1995) and Maeder (1992) for solar and subsolar metallicities. The yields of M92 and WW95C are consistent at low metallicities, but for solar metallicities their yields diverge for high mass stars due to the inclusion of mass loss via stellar winds in the M92 models.

Fig. 2.— The evolution of gas mass (M_g; solid line), stellar mass (M_S; dashed line), total mass (M_T; dash–dot–dot–dot line), and metallicity (dash–dot line) as a function of age for a typical closed box model (Run 1). The mass in stellar remnants is $M_r = M_T - M_g - M_S$.

Fig. 3.— The evolution of gas mass (solid line), stellar mass (dashed line), total mass (dash–dot–dot–dot line), and metallicity (dash–dot line) as a function of age for a typical infall model (Run 11).

Fig. 4.— The evolution of gaseous metals (ZM_g) for different star formation rate parameters. These curves are derived using the yields of M92 ($m_u = 120\,M_\odot$), using $x = 1.35$, and with no infall (closed box models).

Fig. 5.— The evolution of gaseous metals as a function of the gas fraction for different IMFs. These curves are solutions of closed box models using the yields of M92. The central group of curves represents all solutions plotted in Figure 4.

Fig. 6.— A comparison of the numerical solutions with the analytical solutions. The upper and lower redshift scales are for numerical solutions of Run 1 and Run 11, which are represented by the upper and lower solid lines, respectively. The analytical closed box solution is the dashed line (eq. [9]) which is similar to the closed box numerical solutions. The analytical simple infall solution is the dotted line (eq. [12]) and is similar to the numerical infall solutions. As $f(t) \rightarrow 0$ the numerical infall solutions approach the closed box solutions. All models predict that the peak of gaseous metals as a fraction of the total mass occurs when approximately 1/2 of the total mass is in stars and 1/2 is in gas. The redshift scales assume $h = 0.8$, $q_o = 0.5$, and $z_f = 5$.

Fig. 7.— The evolution of the C/O ratio as a function of metallicity for different stellar yields, where the boxes represent abundance measurements of HII galaxies, the diamonds are for halo stars and the triangles are for disk stars. All curves use $x = 1.35$, $\nu = 2$, $n = 1.5$, and $\tau_f = 0$. The stellar yields of M92 better fit the observed increase of the C/O ratio with metallicity and indicate the significance of stellar winds from massive stars which were neglected in the WW95 models.

Fig. 8.— The variation of the C/O ratio as a function of metallicity for different star formation rates, IMFs, and infall parameters using the yields of M92. The boxes, diamonds, and triangles represent the same observations shown in Figure 7.

Fig. 9.— Fits to the molecular cloud abundances. The data points are gas–phase steady–state solutions for the dark cloud models of LG89. These data demonstrate that the abundances are extremely sensitive to the gas phase C/O ratio.

Fig. 10.— The O_2/CO ratio as a function of the O/C ratio. The 2σ observational upper limits of the O_2/CO ratio are shown along with their estimated uncertainties of the O/C ratio. The theoretical data are from many different time dependent molecular chemistry models. For O/C$\gtrsim 10$ the solutions at early times converge with the steady–state solutions. Molecular clouds may be described by the early–time solutions which could result from turbulent mixing of the gas and may explain the apparent lack of O_2 at solar abundances [$(O/C)_\odot \simeq 2$].

Fig. 11.— The evolution of the gas–phase steady–state O_2/CO abundance ratio within dark molecular clouds ($A_V \gtrsim 5$) as a function of age for all models.

Fig. 12.— The evolution of the gas–phase steady–state O_2/CO abundance ratio within dark molecular clouds as a function of metallicity for all models.

Fig. 13.— The evolution of the global volume–weighted O_2/CO abundance ratio corrected for photodissociation effects as a function of metallicity and the SFR (see text). The solid line represents the uncorrected steady–state solutions which are only applicable for dark molecular clouds. Run 1 and Run 13 are closed box models using the stellar yields of M92 and WW95C, respectively. Run 10 and Run 22 are infall models using the stellar yields of M92 and WW95C, respectively.

Fig. 14.— The evolution of the dust, CO, and O_2 (short–dashed lines) masses as a function of metallicity. The models are the same as those shown in Figure 13. The three scenarios for the evolution of O_2 (volume–weighted abundances corrected for photodissociation effects) are labeled as (a) steady state, (b) early times, and (c) selective O depletion (see text).

Fig. 15.— The evolution of the dust mass (long–dashed line), CO mass (solid line), and O_2 mass (short–dashed lines) as a function of the gas fraction. The models are the same as those shown in Figure 14. The redshift scales assume $h = 0.8$, $q_o = 0.5$, and $z_f = 5$.

Fig. 16.— The evolution of the thermal dust continuum emission observed at 240 GHz (1.25 mm) as a function of redshift for galaxies with a final total baryonic mass of $10^{12}\,M_\odot$ and dust temperatures of 40 K and 20 K (eq. [34]). The solid lines are calculations for the same evolutionary models and cosmological parameters used in Figure 15. The dashed lines represent nonevolutionary scenarios with a dust mass achieved at $t = 10$ Gyr in their corresponding numerical model.

Fig. 17.— The evolution of the strengths of the CO(1→0) and $O_2(1,1 \rightarrow 1,0)$ line intensities as a function of redshift for galaxies with a final total baryonic mass of $10^{12}\,M_\odot$ and with a FWHM line width of 300 km s^{-1}. The calculations are for the same evolutionary models and cosmological parameters used in Figure 15. The nonevolutionary scenarios (CO n.e.; long–dashed lines) are for the total mass of the CO emission regions achieved at $t = 10$ Gyr in their corresponding numerical model.

TABLE 1
MODEL PARAMETERS

Run	x	m_u $M_\odot$	α	ν $(10^9\mathrm{yr})^{-1}$	n	τ_f 10^9yr	Stellar Yields
	(1)	(2)	(3)	(4)	(5)	(6)	(7)
1	1.35	120	1.5	2.0	1.5	0	M92
2	1.10	120	1.5	2.0	1.5	0	M92
3	1.70	120	1.5	2.0	1.5	0	M92
4	1.35	40	1.5	2.0	1.5	0	M92
5	1.35	120	0	2.0	1.5	0	M92
6	1.35	120	1.5	5.0	1.5	0	M92
7	1.35	120	1.5	0.5	1.5	0	M92
8	1.35	120	1.5	2.0	1.0	0	M92
9	1.35	120	1.5	2.0	2.0	0	M92
10	1.35	120	1.5	2.0	1.5	1	M92
11	1.35	120	1.5	2.0	1.5	2	M92
12	1.35	120	1.5	2.0	1.5	4	M92
13	1.35	40	1.5	2.0	1.5	0	WW95C
14	1.35	40	1.5	2.0	1.5	0	WW95B
15	1.10	40	1.5	2.0	1.5	0	WW95C
16	1.70	40	1.5	2.0	1.5	0	WW95C
17	1.35	40	0	2.0	1.5	0	WW95C
18	1.35	40	1.5	5.0	1.5	0	WW95C
19	1.35	40	1.5	0.5	1.5	0	WW95C
20	1.35	40	1.5	2.0	1.0	0	WW95C
21	1.35	40	1.5	2.0	2.0	0	WW95C
22	1.35	40	1.5	2.0	1.5	1	WW95C
23	1.35	40	1.5	2.0	1.5	2	WW95C
24	1.35	40	1.5	2.0	1.5	4	WW95C

(1)IMF slope $\Phi \propto m^{-(1+x)}$.
(2)Upper stellar mass limit.
(3)Mixing length parameter.
(4)SFR efficiency, $SFR = \nu M_T (M_g/M_T)^n$.
(5)Exponent to SFR power law.
(6)Infall time constant, $f(t) = (10^{12} M_\odot/\tau_f)\exp(-t/\tau_f)$.
(7)Adopted stellar yields (see text).

TABLE 2
MODEL CONSTRAINTS

Run	Yield y_z (1)	B (2)	O/C *Low* (3)	$Z/Z_\odot$ (10^{10}yr) (4)	$\log(M_g/M_t)$ (10^{10}yr) (5)	Code (6)
1	0.025	0.31	10.13	5.00	-1.81	.2...
2	0.067	0.40	15.96	12.80	-1.59	1.34.
3	0.006	0.41	6.36	1.26	-1.97	1....
4	0.015	0.18	3.95	3.18	-1.84	.23..
5	0.025	0.38	10.13	4.98	-1.81	.....
6	0.024	0.39	13.51	6.40	-2.48	..345
7	0.026	0.27	8.02	2.65	-0.91	.2..5
8	0.024	0.33	10.70	11.05	-4.93	.2.45
9	0.025	0.31	10.12	3.38	-1.19	.2...
10	0.024	0.39	9.55	3.83	-1.65	.....
11	0.024	0.40	9.55	2.43	-1.38	.....
12	0.023	0.40	9.56	1.61	-1.11	.....
13	0.014	0.06	5.77	2.90	-1.84	.23..
14	0.013	0.04	5.37	2.77	-1.84	.23..
15	0.035	0.02	6.47	5.50	-1.67	.2.4.
16	0.003	0.47	4.96	0.87	-1.98	1.34.
17	0.014	0.31	5.22	2.88	-1.84	.23..
18	0.013	0.03	6.14	3.55	-2.50	.2..5
19	0.015	0.17	5.54	1.62	-0.94	.23.5
20	0.014	0.04	5.79	5.30	-5.04	.2345
21	0.014	0.07	5.76	2.04	-1.20	.23..
22	0.014	0.12	5.91	2.32	-1.67	.23..
23	0.013	0.13	5.89	1.51	-1.40	.23..
24	0.013	0.14	5.91	1.02	-1.12	.23..

(1) Implied net yields from analytical solutions.
(2) $B \propto \log(C/O)/\log(O/H)$.
(3) O/C ratio at $\log(O/H) = -4.64$.
(4) Metallicity at 10 Gyr.
(5) Gas fraction at 10 Gyr.
(6) The numbers indicate values of the model parameters given in columns (1–5) which are outside of the acceptable range for current spiral galaxies, while the "dots" indicate values consistent with the model constraints.

TABLE 3
IMPORTANT EPOCHS

Run	$\tau^*_{1/2}$ (GYr) (1)	$(ZM_g)_{max}$ (GYr) (2)	$Z_\odot$ (GYr) (3)
1	0.496	0.774	0.592
2	0.632	1.070	0.232
3	0.436	0.790	5.600
4	0.478	0.808	1.150
5	0.496	0.762	0.598
6	0.194	0.328	0.246
7	2.090	3.030	2.330
8	0.412	0.574	0.484
9	0.608	0.986	0.734
10	1.570	2.100	1.530
11	2.470	3.110	1.970
12	4.100	4.400	2.470
13	0.480	0.864	1.230
14	0.478	0.868	1.310
15	0.562	0.956	0.474
16	0.432	0.858	> 10.2
17	0.480	0.894	1.250
18	0.188	0.380	0.506
19	2.010	3.520	4.840
20	0.398	0.656	0.856
21	0.584	1.180	1.900
22	1.550	2.150	3.150
23	2.440	3.160	4.920
24	4.070	4.430	9.370

(1) Age when 1/2 of the final total mass is in stars or stellar remnants.
(2) Age when the amount of gaseous metals is maximum.
(3) Age when the metallicity is solar.

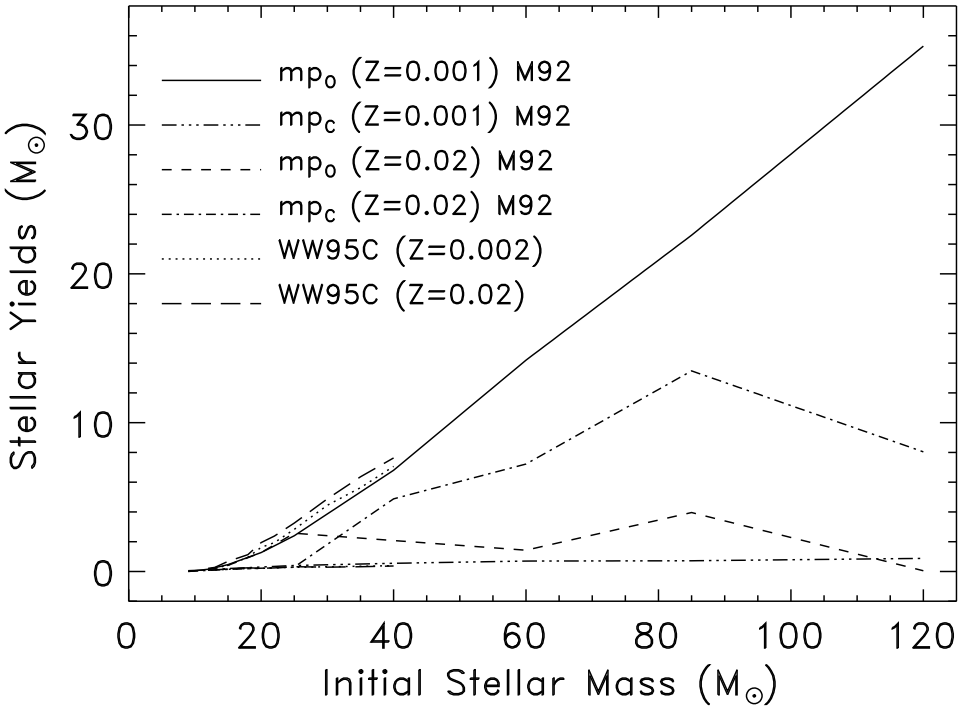
mp$_o$ (Z=0.001) M92
mp$_c$ (Z=0.001) M92
mp$_o$ (Z=0.02) M92
mp$_c$ (Z=0.02) M92
WW95C (Z=0.002)
WW95C (Z=0.02)
Stellar Yields (M$_\odot$)
Initial Stellar Mass (M$_\odot$)
0
10
20
30
0
20
40
60
80
100
120

Fig. 1.—

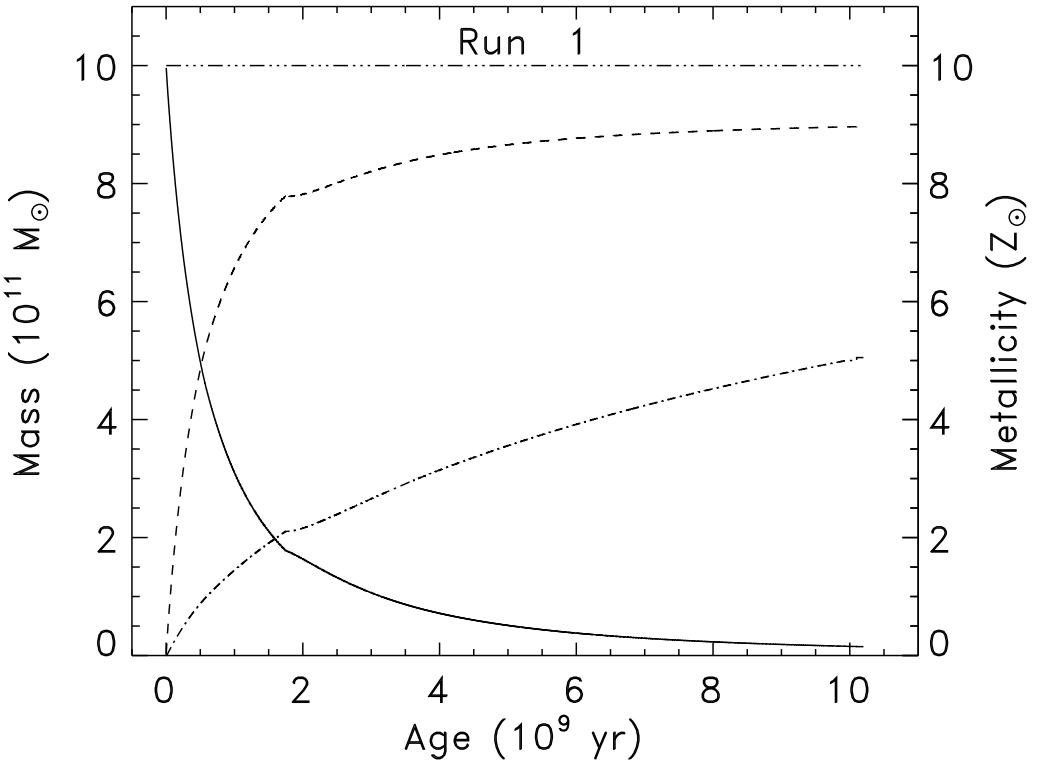

Fig. 2.—

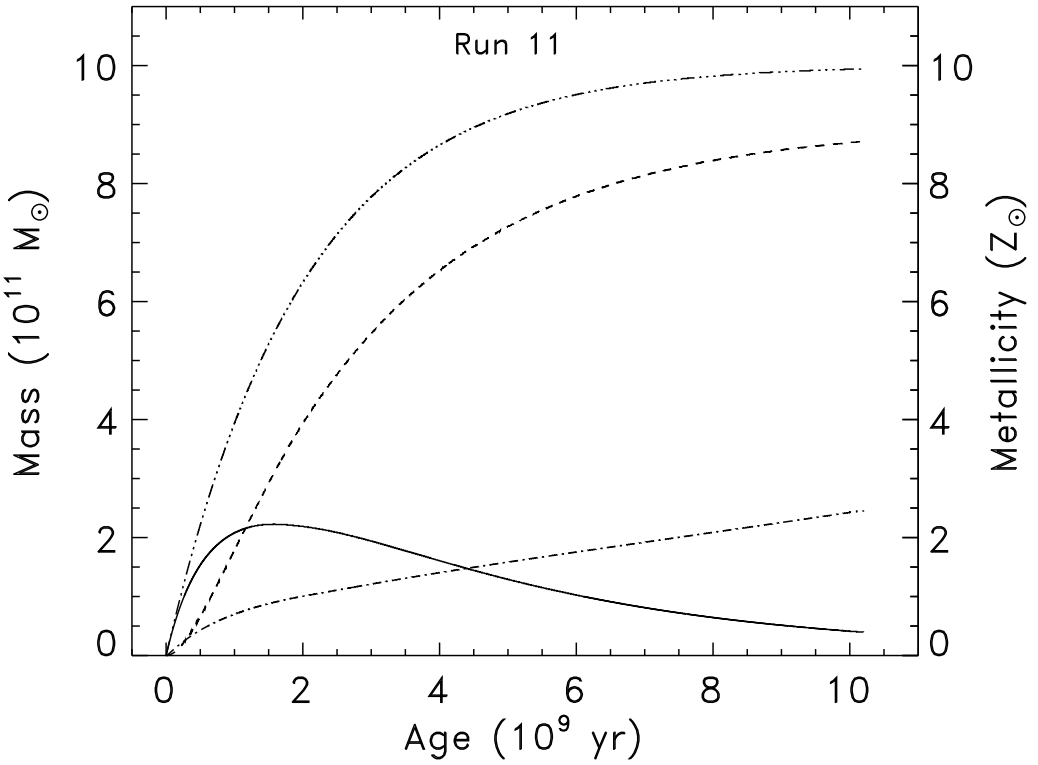

Fig. 3.—

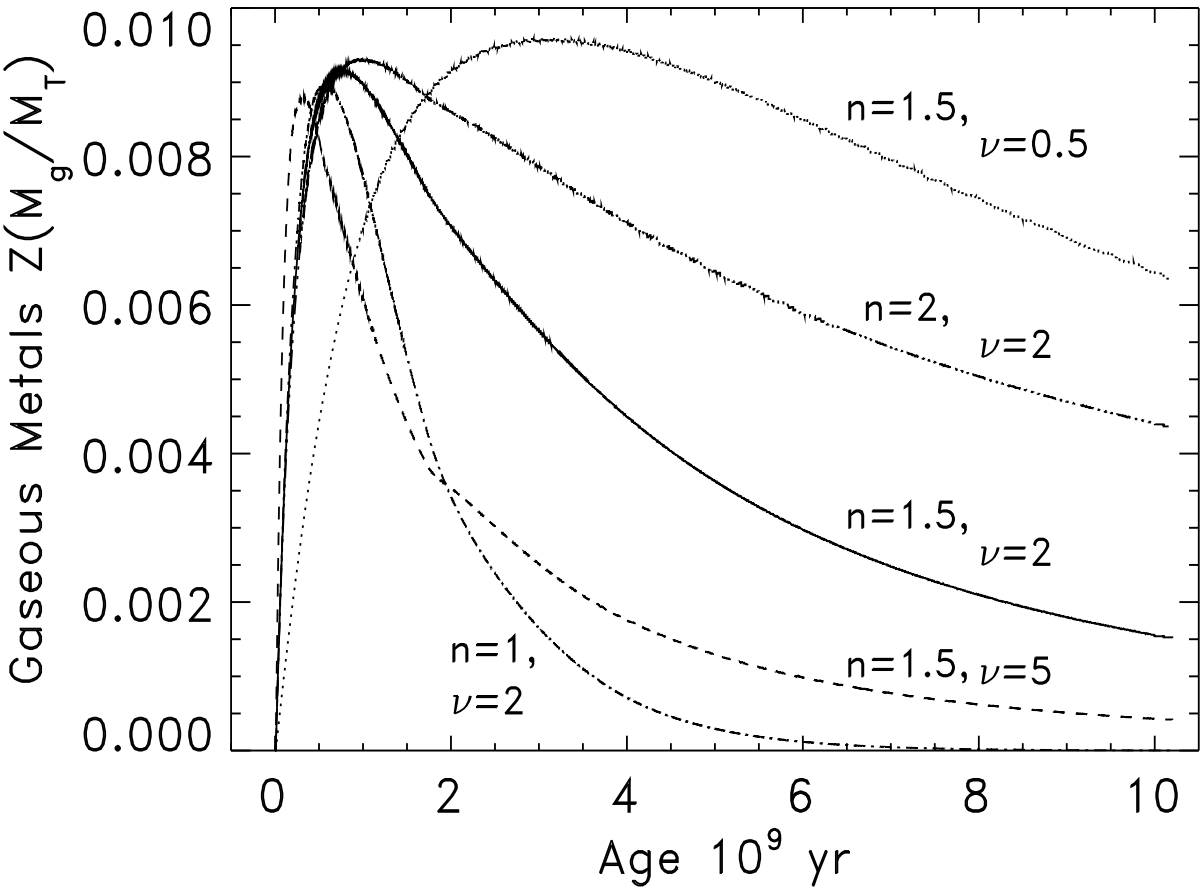
0.010
0.008
0.006
0.004
0.002
0.000
Gaseous Metals Z(M_g/M_T)
0
2
4
6
8
10
Age 10^9 yr
n=1.5, ν=0.5
n=2, ν=2
n=1.5, ν=2
n=1.5, ν=5
n=1, ν=2

Fig. 4.—

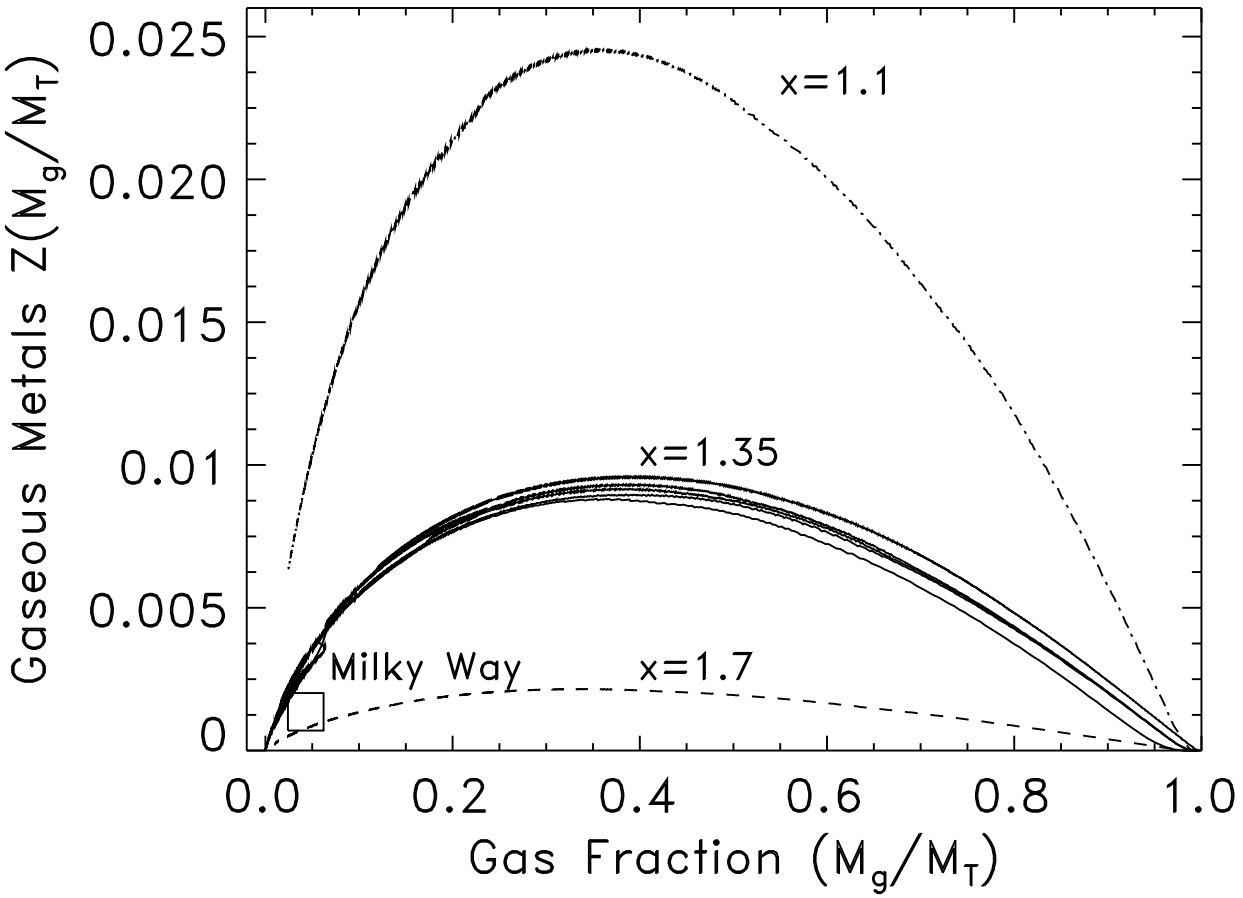
0.025
0.020
0.015
0.01
0.005
0
Gaseous Metals Z(M_g/M_T)
x=1.1
x=1.35
x=1.7
Milky Way
0.0
0.2
0.4
0.6
0.8
1.0
Gas Fraction (M_g/M_T)

Fig. 5.—

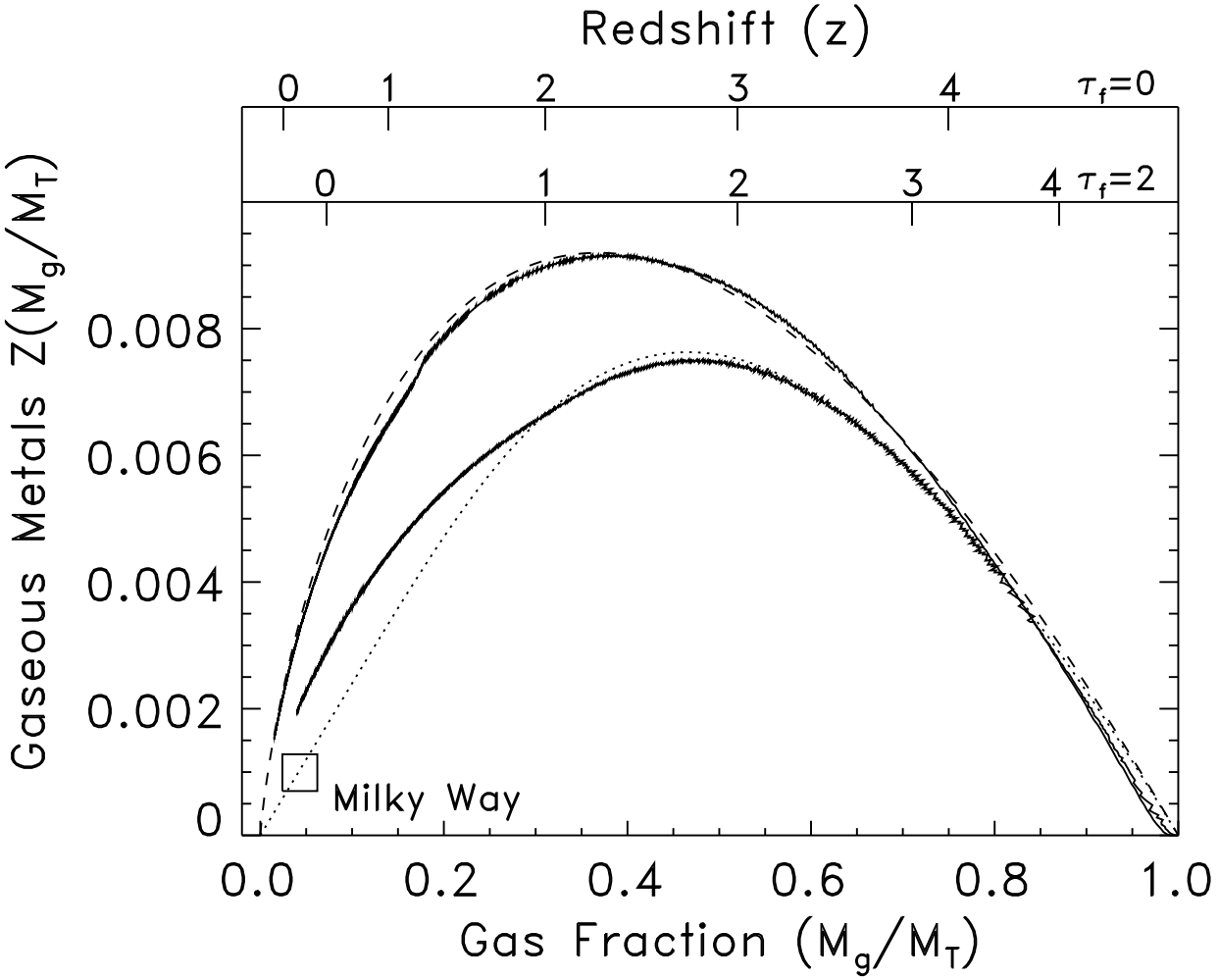
Redshift (z)
0
1
2
3
4
τ_f=0
0
1
2
3
4
τ_f=2
Gaseous Metals Z(M_g/M_T)
0.008
0.006
0.004
0.002
0
Milky Way
0.0
0.2
0.4
0.6
0.8
1.0
Gas Fraction (M_g/M_T)

Fig. 6.—

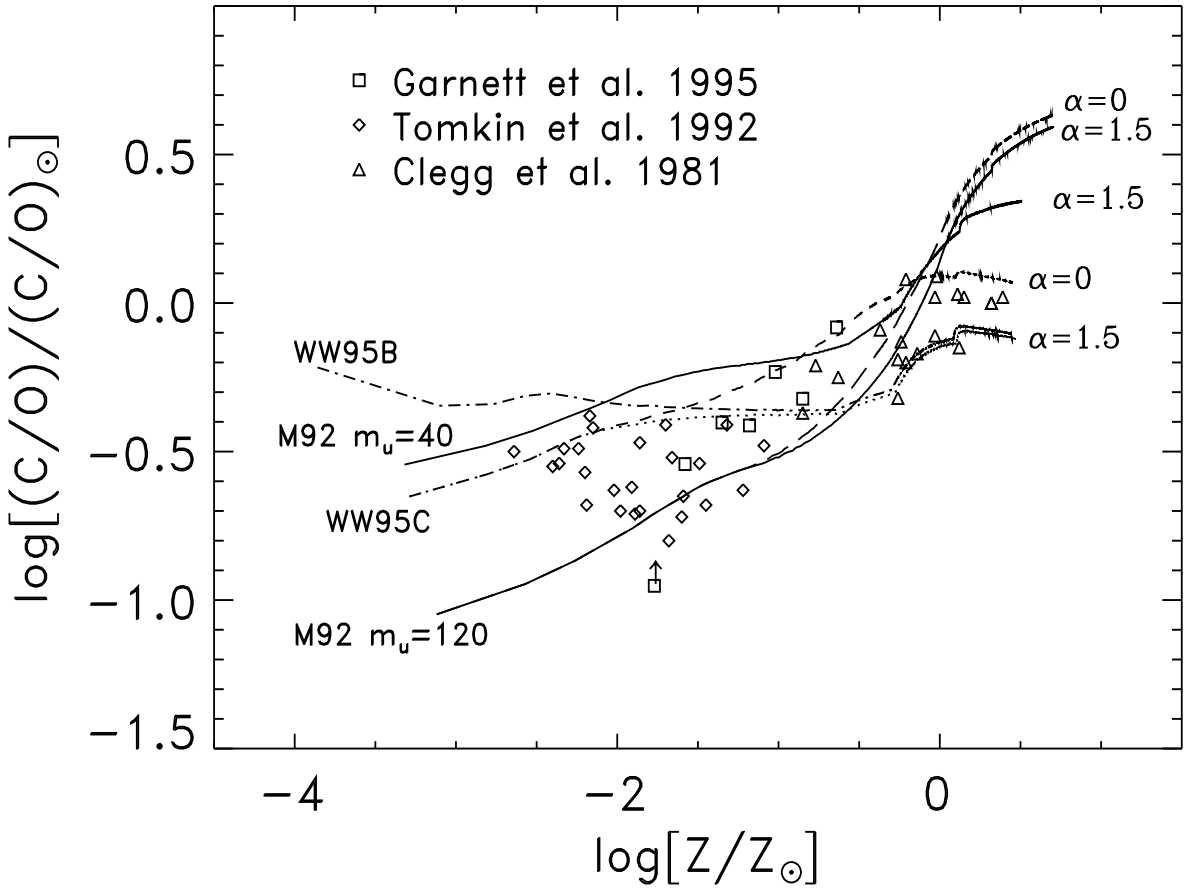
Garnett et al. 1995
Tomkin et al. 1992
Clegg et al. 1981
α=0
α=1.5
α=1.5
α=0
α=1.5
WW95B
M92 m_u=40
WW95C
M92 m_u=120
0.5
0.0
−0.5
−1.0
−1.5
−4
−2
0
log[(C/O)/(C/O)⊙]
log[Z/Z⊙]

Fig. 7.—

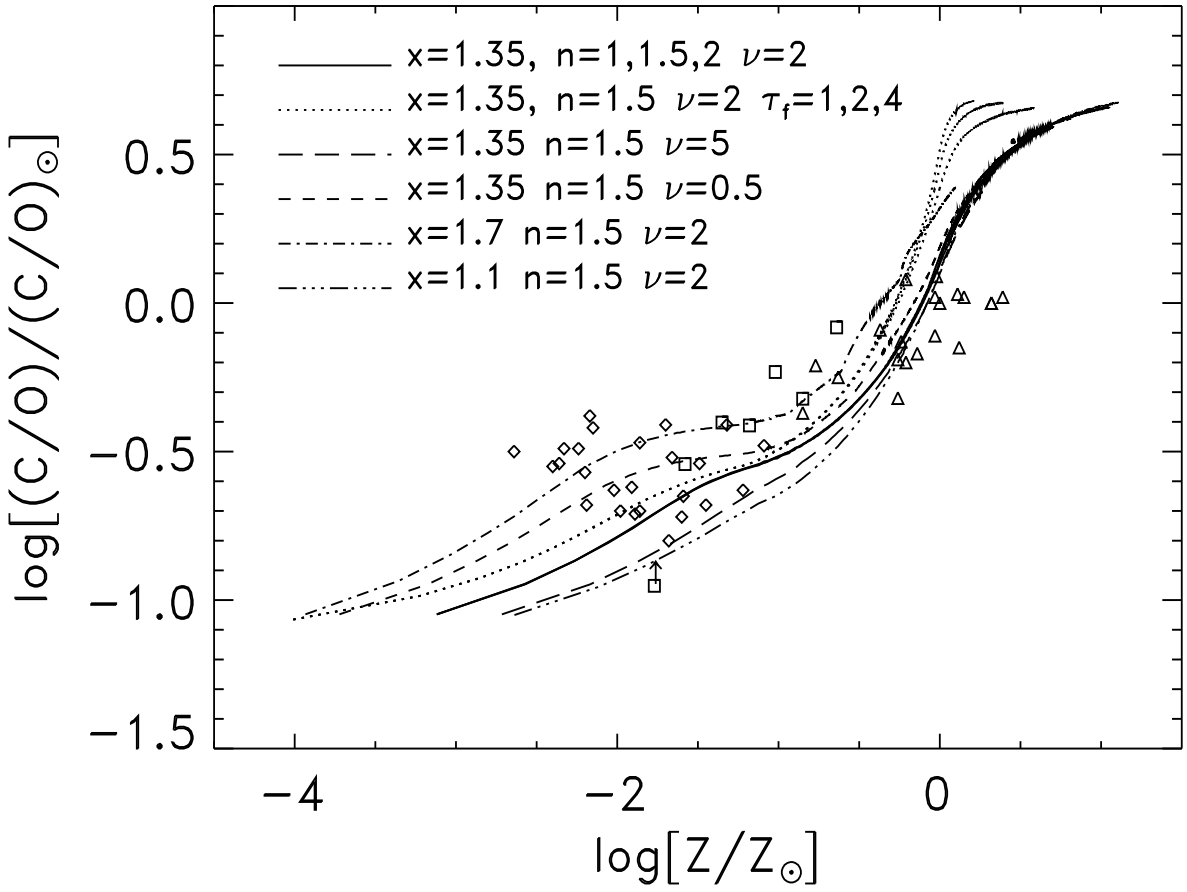
x=1.35, n=1,1.5,2 ν=2
x=1.35, n=1.5 ν=2 τf=1,2,4
x=1.35 n=1.5 ν=5
x=1.35 n=1.5 ν=0.5
x=1.7 n=1.5 ν=2
x=1.1 n=1.5 ν=2
log[(C/O)/(C/O)⊙]
log[Z/Z⊙]
0.5
0.0
−0.5
−1.0
−1.5
−4
−2
0

Fig. 8.—

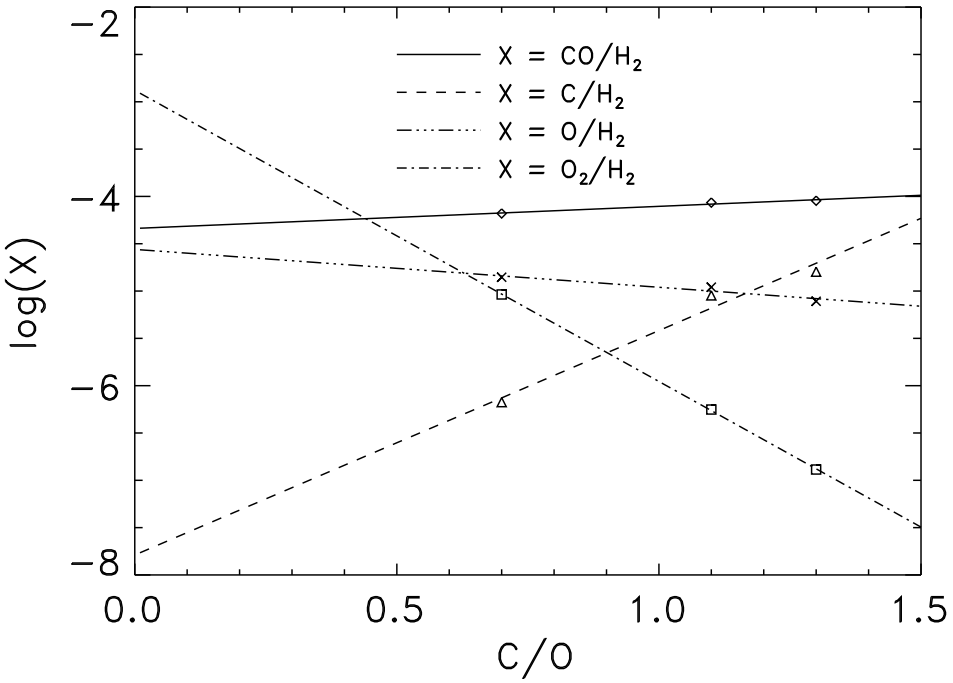

Fig. 9.—

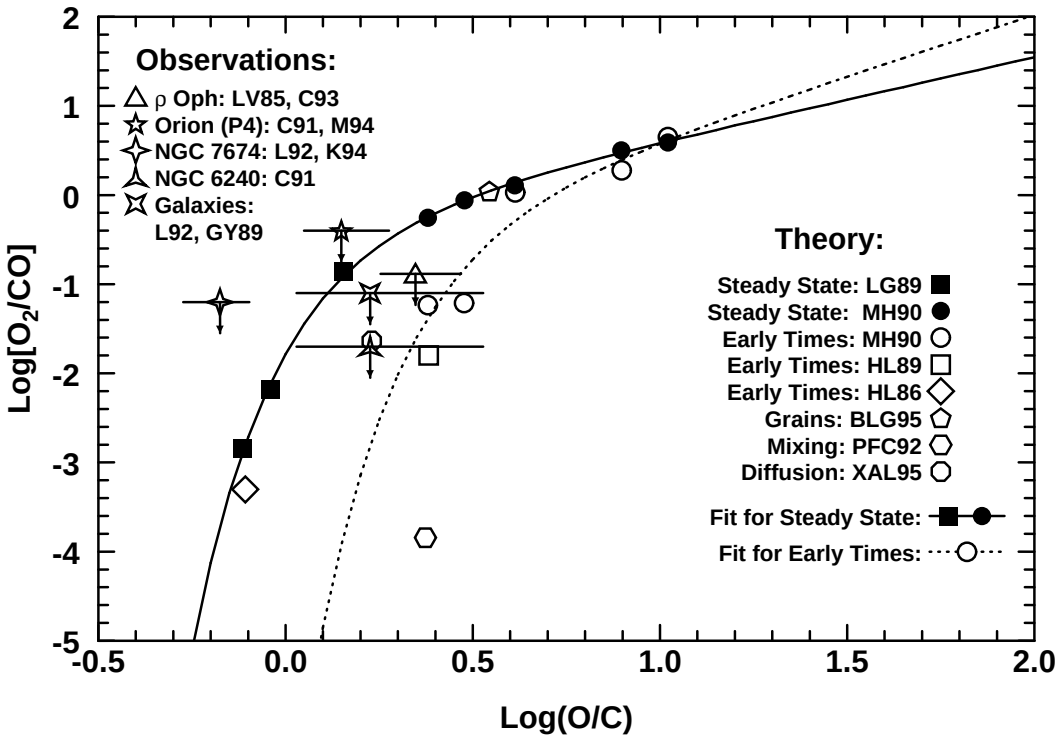
Observations:
ρ Oph: LV85, C93
Orion (P4): C91, M94
NGC 7674: L92, K94
NGC 6240: C91
Galaxies:
L92, GY89
Theory:
Steady State: LG89
Steady State: MH90
Early Times: MH90
Early Times: HL89
Early Times: HL86
Grains: BLG95
Mixing: PFC92
Diffusion: XAL95
Fit for Steady State:
Fit for Early Times:
Log[O2/CO]
Log(O/C)
2
1
0
-1
-2
-3
-4
-5
-0.5
0.0
0.5
1.0
1.5
2.0

Fig. 10.—

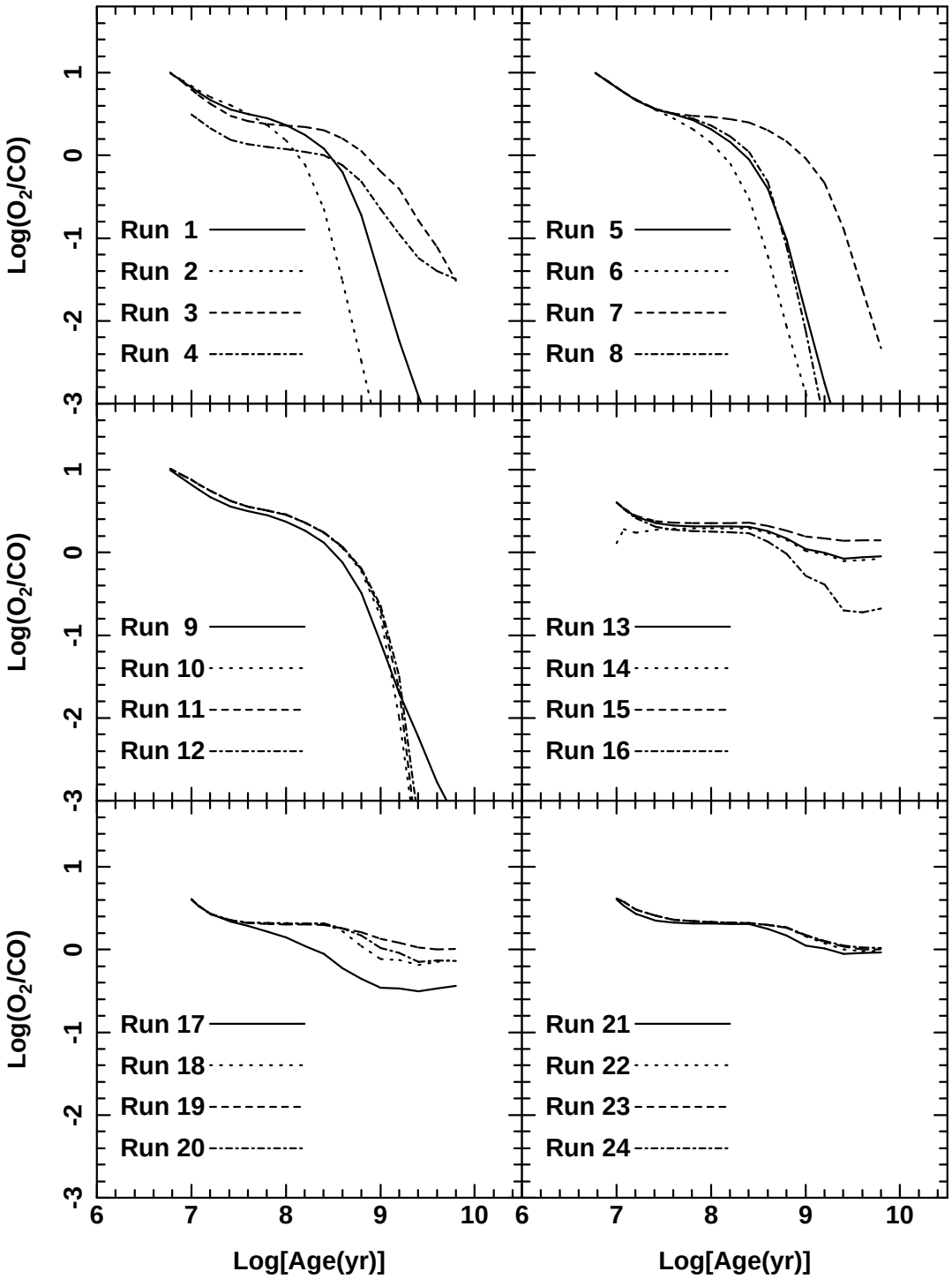
Log(O2/CO)
Log[Age(yr)]
Run 1
Run 2
Run 3
Run 4
Run 5
Run 6
Run 7
Run 8
Run 9
Run 10
Run 11
Run 12
Run 13
Run 14
Run 15
Run 16
Run 17
Run 18
Run 19
Run 20
Run 21
Run 22
Run 23
Run 24

Fig. 11.—

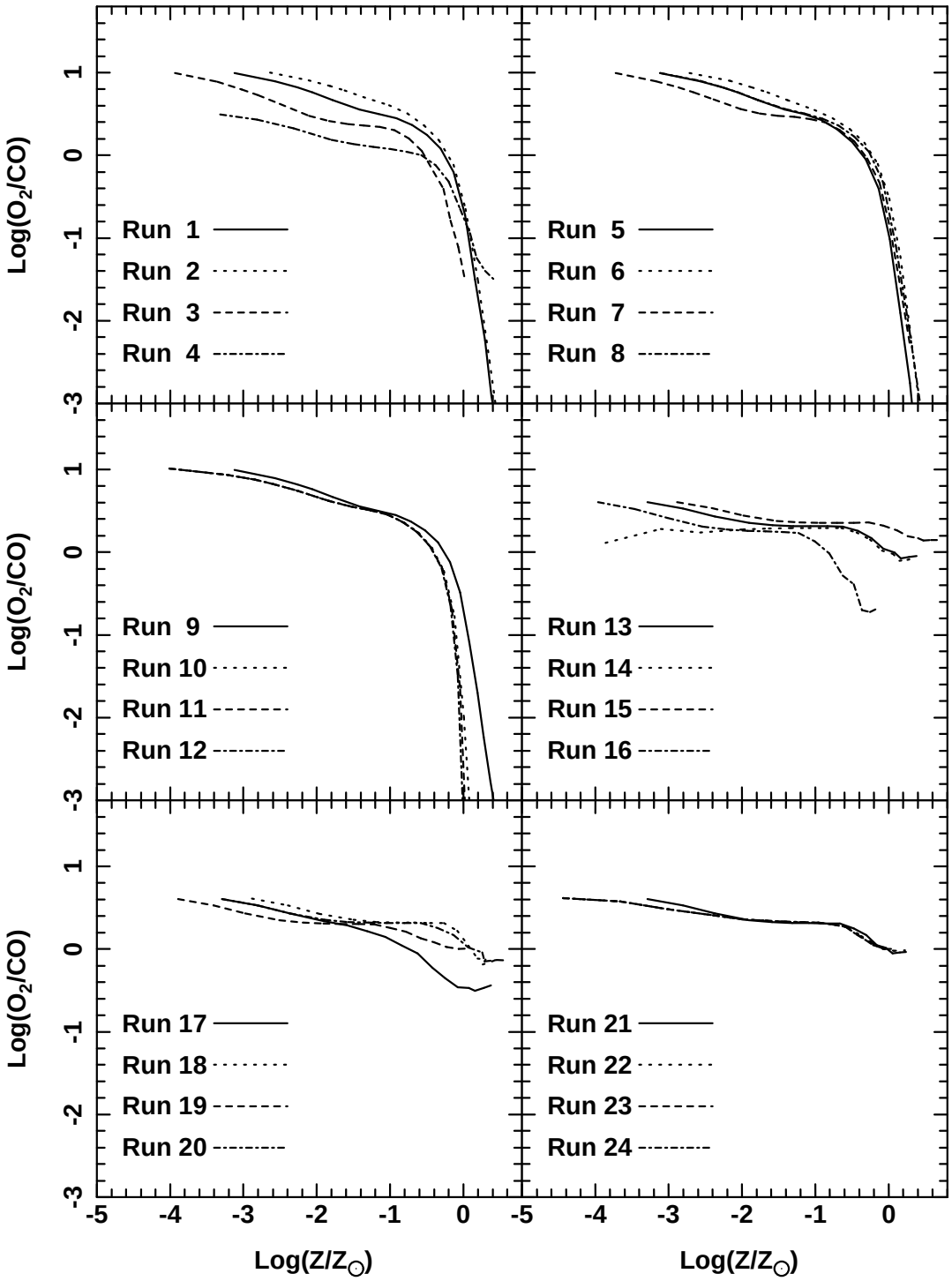
Log(O2/CO)
Log(Z/Z⊙)
Run 1
Run 2
Run 3
Run 4
Run 5
Run 6
Run 7
Run 8
Run 9
Run 10
Run 11
Run 12
Run 13
Run 14
Run 15
Run 16
Run 17
Run 18
Run 19
Run 20
Run 21
Run 22
Run 23
Run 24

Fig. 12.—

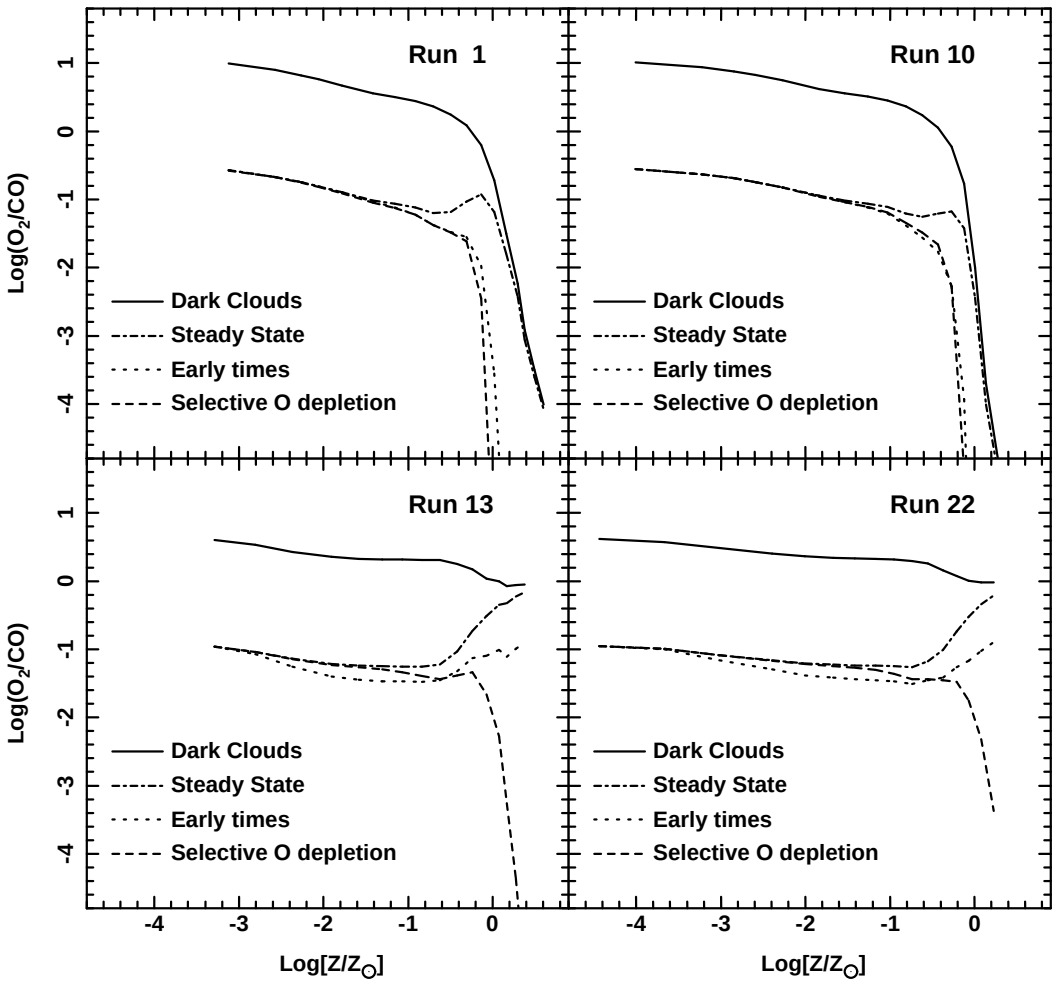
Run 1
Run 10
Run 13
Run 22
Dark Clouds
Steady State
Early times
Selective O depletion
Log(O2/CO)
Log[Z/Z⊙]
1
0
-1
-2
-3
-4

Fig. 13.—

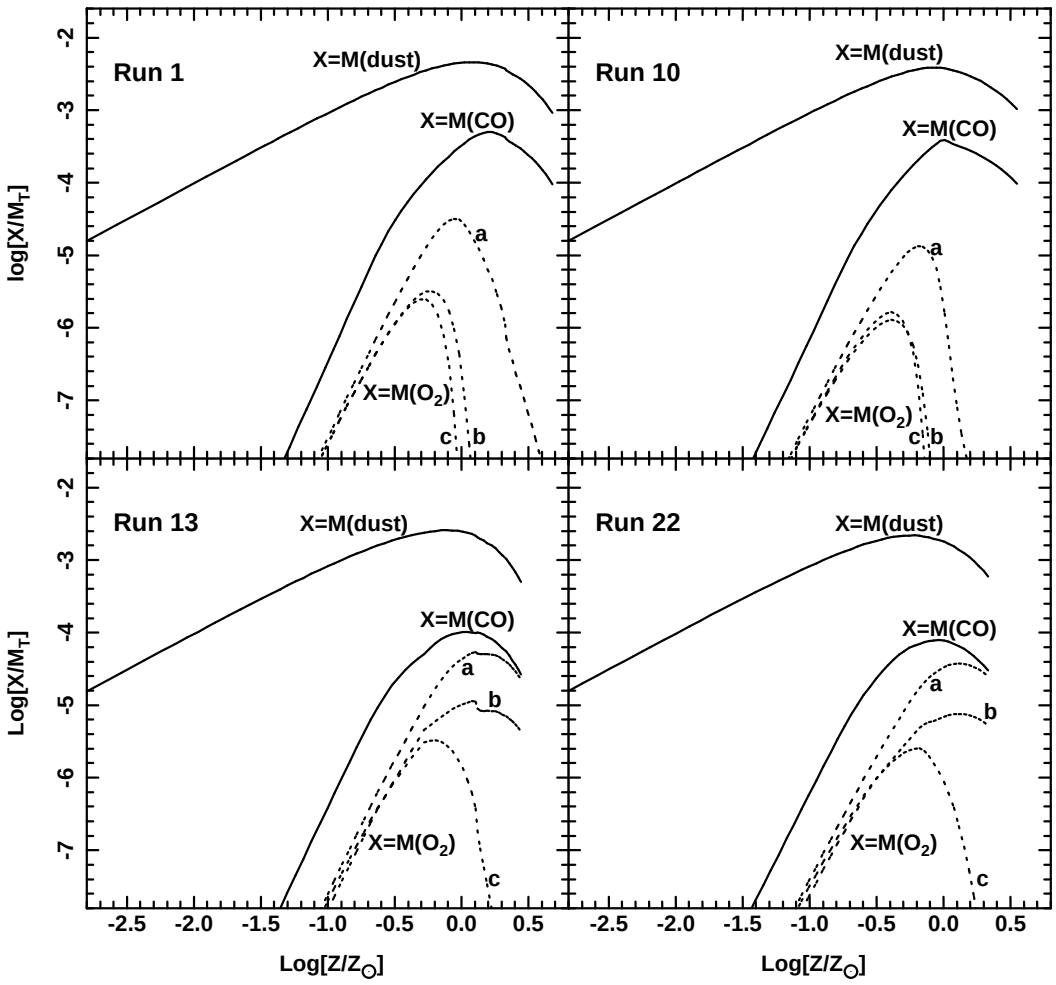
Run 1
X=M(dust)
X=M(CO)
a
X=M(O2)
c
b
Run 10
X=M(dust)
X=M(CO)
a
X=M(O2)
c
b
Run 13
X=M(dust)
X=M(CO)
a
b
X=M(O2)
c
Run 22
X=M(dust)
X=M(CO)
a
b
X=M(O2)
c
log[X/MT]
Log[X/MT]
-2
-3
-4
-5
-6
-7
-2.5
-2.0
-1.5
-1.0
-0.5
0.0
0.5
Log[Z/Z⊙]

Fig. 14.—

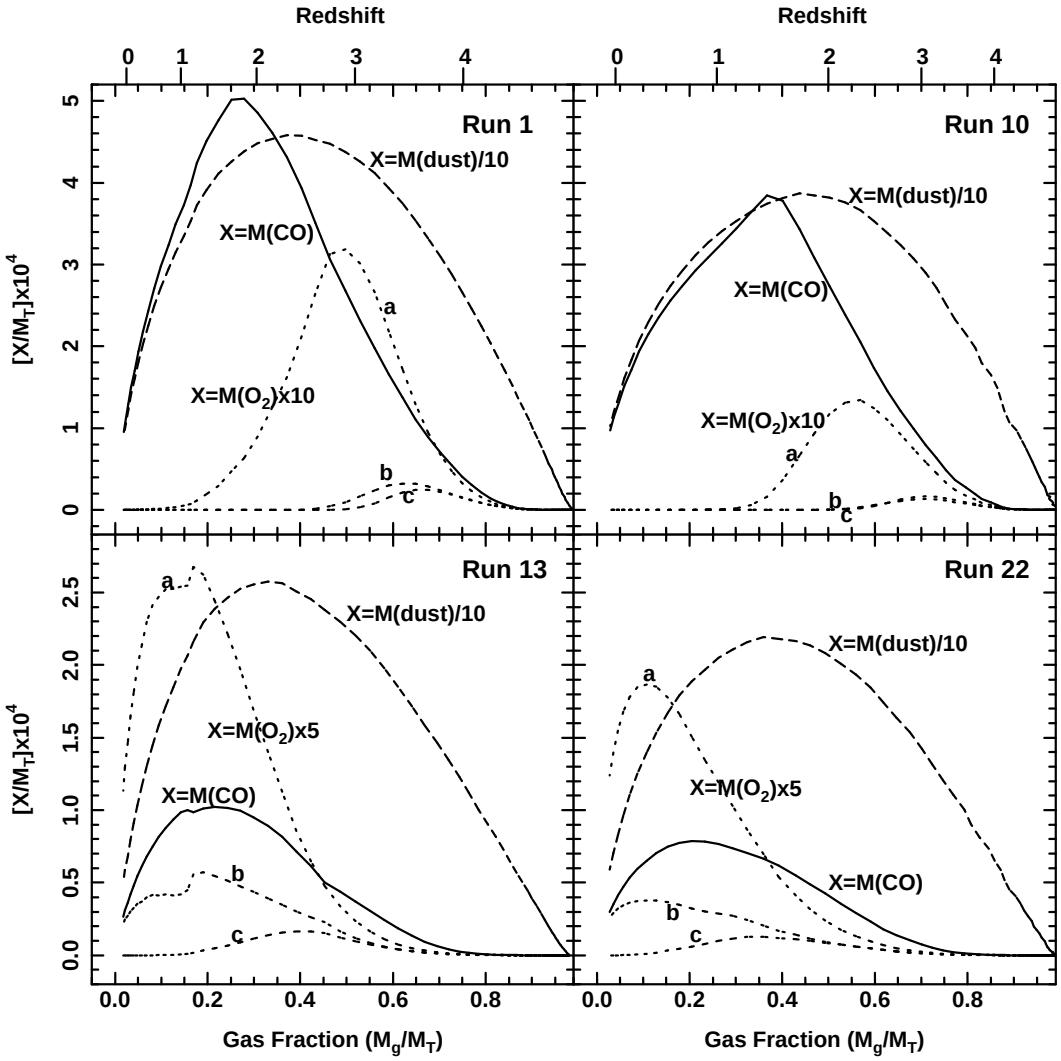
Redshift
Redshift
Run 1
Run 10
Run 13
Run 22
X=M(dust)/10
X=M(CO)
X=M(O2)x10
X=M(O2)x5
a
b
c
[X/MT]x10^4
Gas Fraction (Mg/MT)

Fig. 15.—

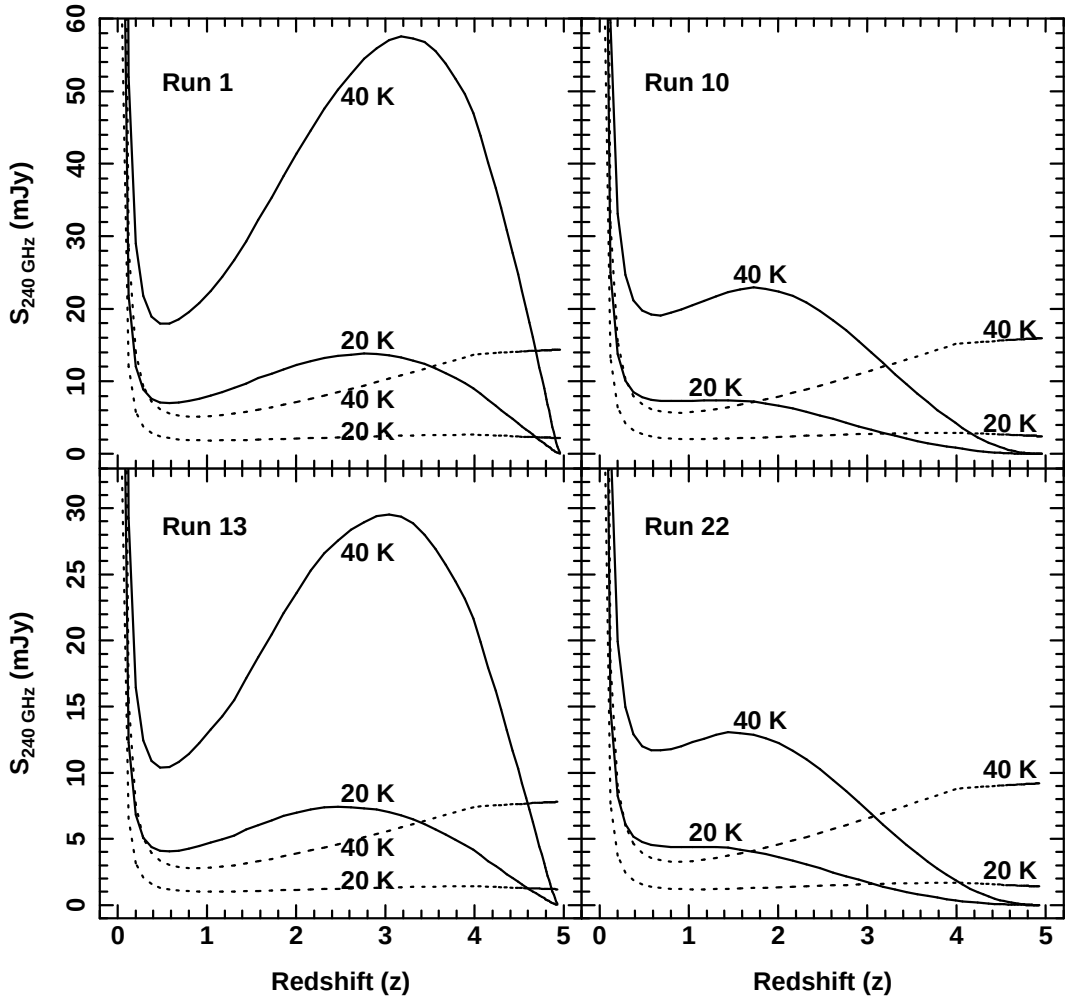
Run 1
40 K
20 K
40 K
20 K
Run 10
40 K
40 K
20 K
20 K
Run 13
40 K
20 K
40 K
20 K
Run 22
40 K
40 K
20 K
20 K
S240 GHz (mJy)
S240 GHz (mJy)
Redshift (z)
Redshift (z)
0
10
20
30
40
50
60
0
5
10
15
20
25
30
0
1
2
3
4
5

Fig. 16.—

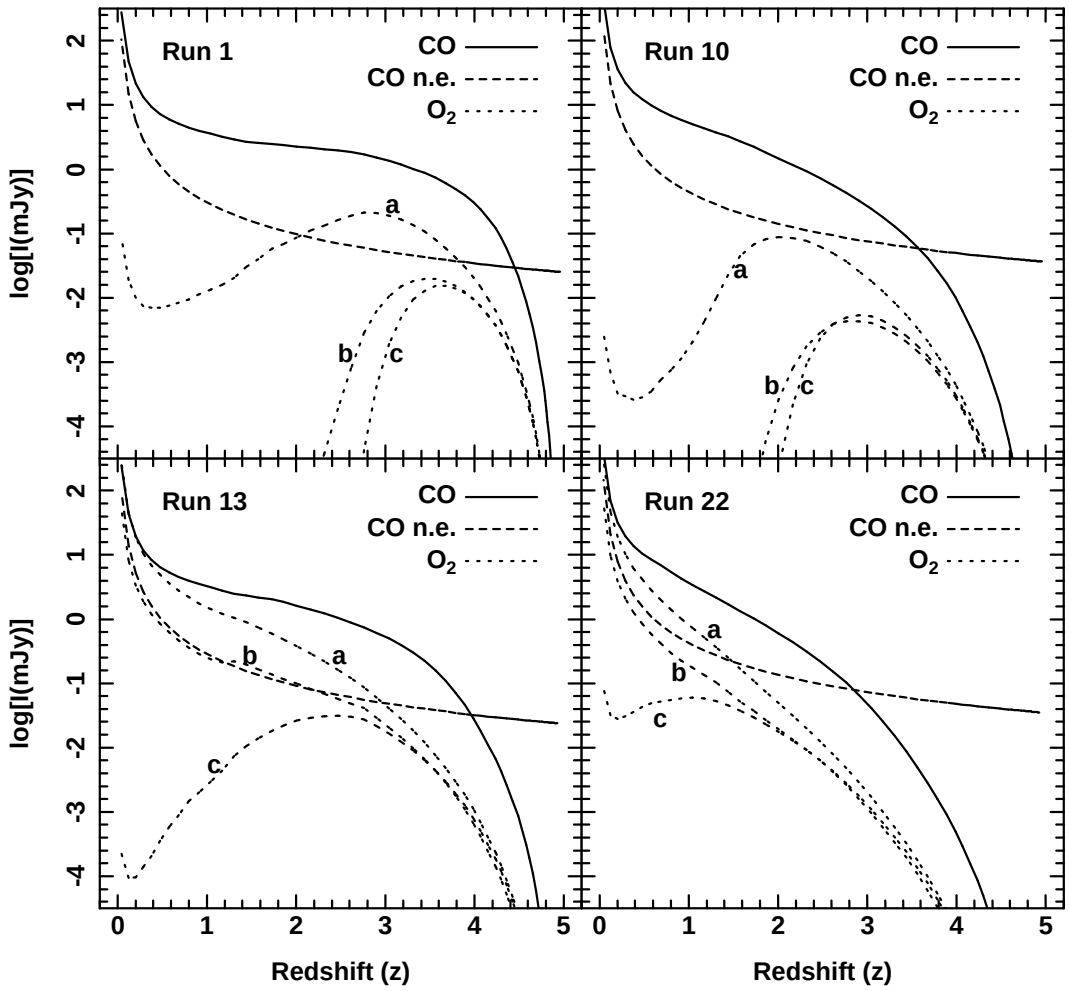

Fig. 17.—